ROSETTA

ROSETTA Radio Science Investigations RSI Gravity field determination from Radio Science Data

Technical Note

Issue: 1.0
Revision: 1.0
Date: 22.03.2018
Document: ROS-RSI-UBW-TN-3141

prepared by

T. Andert

approved by

Martin Pätzold
(RSI Principal Investigator)

page left free

Contents

List of Figures

List of Tables

Acronyms

AU Astronomical Unit

CEP Celestial Ephemeris Pole

DSN Deep Space Network

EOPs Earth Orientation Parameters

ESA European Space Agency

ET Ephemeris Time

GAST Greenwich Apparent Sidereal Time

GMST Greenwich Mean Sidereal Time

GPS Global Positioning System Time

ITRF International Terrestrial Reference Frame

JPL Jet Propulsion Laboratory

LOD Length of Day

MEX Mars Express

ROS Rosetta

SVD Singular Value Decomposition

SPICE Information system to assist scientists in planning and interpreting scientific observations from space-based instruments (see *NAIF* [2009])

TAI International Atomic Time

TCB Barycentric Coordinate Time

TCG Geocentric Coordinate Time

TDB Barycentric Dynamic Time

TSAC Tracking System Analytic Calibration

TDT Terrestrial Dynamic Time

TT Terrestrial Time

UT1 Universal Time

UTC Coordinated Universal Time

CHAPTER 1

Introduction

The following document describes the theoretical background how to extract the gravity field of a solar system body from radio tracking data. The document is designed to serve as a starting point to develop a software package which is able to extract the gravity field from Radio Science data. It does not claim completeness but provides a solid background knowledge.

The Radio Science experiment technique enables the precise estimation of the mass and additional gravitational parameters of solar system bodies. It uses the radio link between ground station and spacecraft. The tracking data contain the frequency of the radio signal observed at the ground station. The observed frequency is proportional to the relative velocity between the spacecraft and the ground station.

The Radio Science measurement principle is based on the detection of a change in frequency of the radio signal. This frequency shift can be caused by the propagation of the radio wave through a medium and/or the change of the relative velocity between the spacecraft and the ground station by an unknown force like the gravitational attraction of a perturbing body (*Häusler* [2002]). For close flybys the latter frequency shift is used for estimating the gravitational parameter of a perturbing body from the trajectory of a spacecraft. Figure 1.1 summarizes the steps needed to be executed to perform precise orbit determination and to obtain gravitational parameters from the measured tracking data.

The precise computation of the predicted frequency expected to be received at the ground station includes appropriate time and coordinate systems for Radio Science experiments which are defined in section 2. A method for solving the equation of motion is described in section 2.4.

A spacecraft orbiting a central body can be perturbed by many forces. These forces

have to be taken into account for a precise orbit determination which is one of the most essential parts in order to extract gravitational parameters from Radio Science data. The gravitational and non-gravitational forces acting on a spacecraft are described in section 3 and 4, respectively. This includes the acceleration caused by a non-spherical shaped body with nonuniform density distribution for which a novel recursion algorithm for normalized gravity coefficients is developed based on an algorithm from *Cunningham* [1970]. The gravitational attractions from third or more bodies are also defined. Detailed models for the solar radiation pressure depending on the optical parameter of the spacecraft and the direction of the normal of each plane of the spacecraft to the Sun and other perturbing forces are specified in detail. Based on the precise orbit determination the predicted frequency which is expected to be received at the ground station is computed from the relativistic Doppler effect. This requires the knowledge of the very accurate position at centimeter level of the transmitting and receiving ground station, i.e. site displacement effects like tectonic plate motion must be taken into account. Numerical methods for modeling this effects and the relativistic Doppler effect are presented in section 5.

The radio signal transmitted from the ground station to the spacecraft and vice versa passes the troposphere and ionosphere of the Earth. The frequency of the signal is changed due to the propagation through these media. Numerical models for predicting and removing this effect from the recorded data are described in section 6.

After applying all corrections, the frequency shift caused by the gravitational attraction of the perturbing body is obtained from the recorded data by subtracting the predicted frequency (all forces are included except the gravitational attraction of the perturbing body) from the recorded frequency.

In section 7 a numerical stable formalism for fitting the gravitational parameter of the body onto the frequency residuals is described. The error of the estimated gravitational parameter is reduced by applying appropriate filter techniques (see section 8).

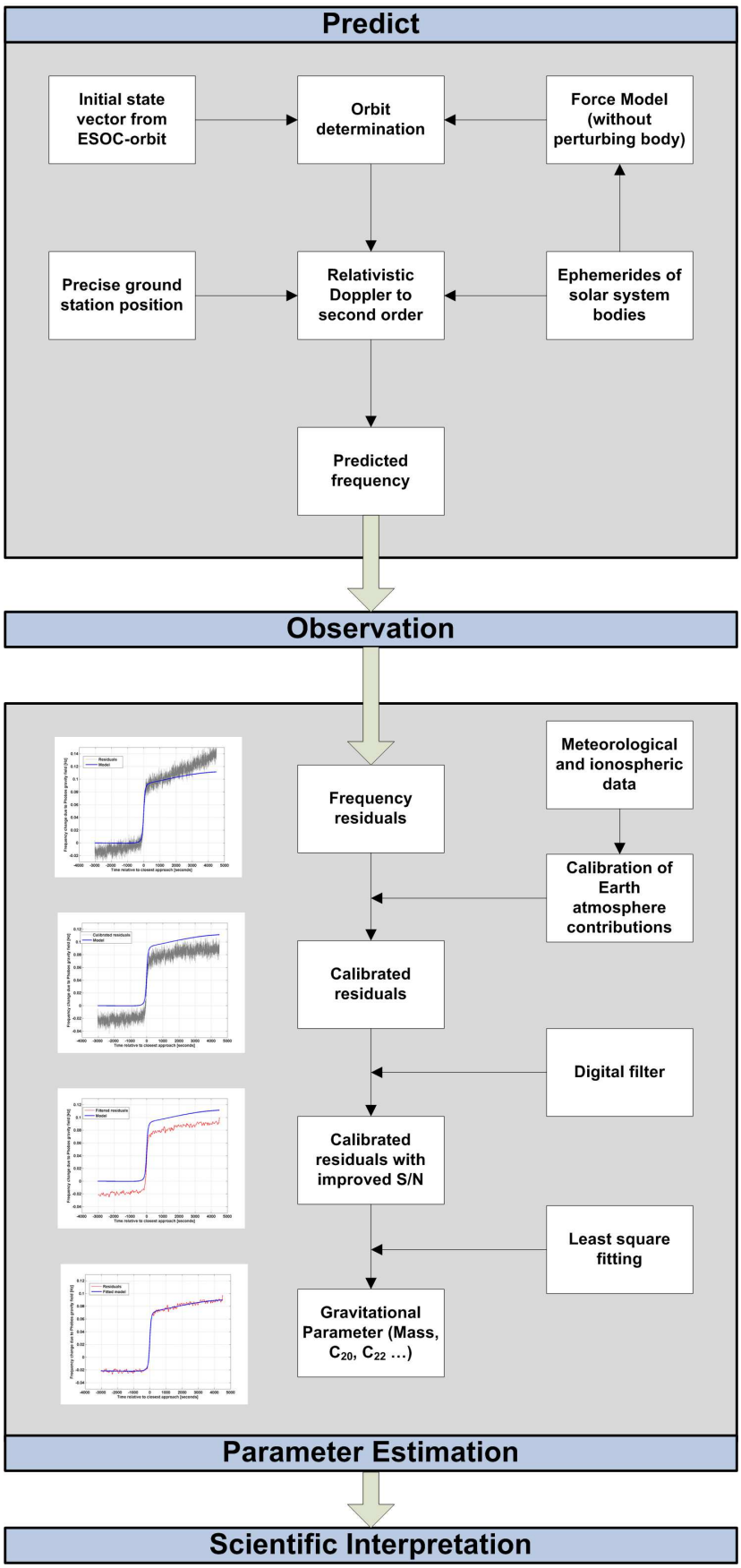

Figure 1.1: *Flow chart describing the major steps of the Radio Science software tool. The uppert part describes the computation of the predicted frequency and the lower part the subtraction of the gravitational parameter including calibration and noise reduction by filtering.*

CHAPTER 2

Time and reference frames

Analyzing data from Radio Science measurements requires a definition of various time systems and reference frames which are suitable for this specific application. Important is, for example, the reference time when the signal transmitted by the spacecraft is received at the ground station.

The software package SPICE (*NAIF* [2009]) used in this thesis provides various built-in time and reference frames and the corresponding transformations between them. The time and reference frames used for the computations are briefly explained in the following.

More information about time and reference frames can be found in *Häusler et al.* [2003], *Selle* [2005], *Montenbruck and Gill* [2000], *Dehant and Mathews* [2007] and *Vallado* [2001].

2.1 Time

The position of the spacecraft and the receiving ground station has to be known very precisely in different time systems. E.g. the position of a planet is based on the Ephemeris Time (ET) and the data recorded at the ground station are referenced to the Coordinated Universal Time (UTC). There are four time scales: sidereal time, solar (universal time), dynamical time, and atomic time. Sidereal time and solar time are based on the rotation of the Earth and are related together by mathematical transformations. Atomic and Dynamical time are not depending on other time scales.

Universal times UT and UT1 are sub timescales of the mean solar time, ET, Terrestrial Time (TT), Barycentric Dynamic Time (TDB), Terrestrial Dynamic Time (TDT),

Barycentric Coordinate Time (TCB) and Geocentric Coordinate Time (TCG) of the dynamical time, and International Atomic Time (TAI) and Global Positioning System Time (GPS) of the atomic time (see Figure 2.1). In this thesis UTC and ET is used.

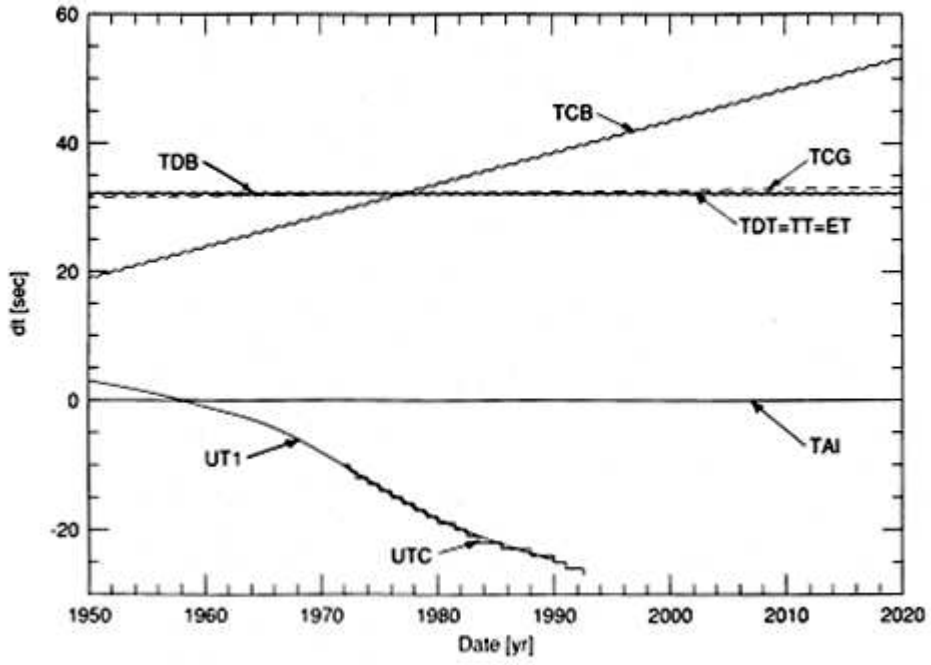

Figure 2.1: *Difference between Barycentric Coordinate Time (TCB), Barycentric Dynamic Time (TDB), Geocentric Coordinate Time (TCG), Terrestrial Time (TT) or former Terrestrial Dynamic Time (TDT), International Atomic Time (TAI), Universal Time (UT1), Global Positioning System Time (GPS) and Coordinated Universal Time (UTC) between 1950 and 2020. The periodic terms of TCB and TDB are magnified by 100 to make them visible (Source: Seidelmann and Fukushima [1992]).*

2.1.1 Coordinated Universal Time

The Coordinated Universal Time (UTC) has a nonuniform time scale and is obtained from atomic clocks which are running at the same rate as TT or former TDT and TAI. TT and TAI have uniform time scales based on atomic clocks which are located at the surface of Earth. UTC is referenced to TAI which has an uniform time scale but due to the introduction of leap seconds the UTC has a nonuniform time scale. This ensures that the UTC time scale is always within 0.7 seconds of UT1. The UT1 represents the time scale of mean solar time with an average length of solar day of 24 hours with UT1 = UT. UT1 takes into account the actual rotation of the Earth. Therefore the length of one second of UT1 is not constant due to the apparent motion of the Sun and the rotation of the Earth (see figure 2.1).

2.1.2 Ephemeris Time

The Ephemeris Time (ET) is the uniform time scale that is represented by the independent variable in the differential equations that describe the motions of the planets, Sun and Moon and is defined as TDB seconds past the Greenwich noon on 1 January 2000 Barycentric Dynamic Time (TDB), below referred to as the `J2000` epoch. ET can be expressed in form of TDB or TDT, but in this thesis the TDB representation is used. It is defined as the basic time system for all computations.

The difference between the UTC and TDB representation is computed from

$$t_{TDB} = t_{UTC} + t_{Leap} + 32.184\,[s] + \Delta t_{TDB,TT}. \tag{2.1}$$

Here t_{Leap} are the leap seconds and $\Delta t_{TDB,TT}$ the difference between TT and TDB.

2.2 Coordinate systems

A coordinate system is usually defined by its origin, fundamental plane, the preferred direction and additionally the sense, or the positive direction. Different coordinate systems are used in the present thesis. Their definition and utilization are below. The names of the coordinate systems are according to the nomenclature from the SPICE software package.

- Geocentric Celestial Reference Frame `J2000`:

  This frame has the Earth mean equator of the J2000 epoch, which is the epoch of Greenwich noon on 1 January 2000 TDB as its principal plane and has no rotation in space. The first axis of this frame is in the direction of the vernal equinox and the second is in the direction of the increasing obliquity. This is the fundamental inertial coordinate system in which the equation of motion of the spacecraft is solved.

- International Terrestrial Reference Frame `ITRF93`:

  This frame is fixed to the Earth, with the center of mass being defined for the entire Earth, including oceans and atmosphere. It is defined through coordinates assigned to a number of sites for which the various effects of site displacement are taken into account. Consequently, the motion of these sites reflects the rotation of the Earth entirely. `ITRF93` has the plane of the true equator as its principal plane and its first axis fixed on the Greenwich meridian. In this frame the precise position of the transmitting and receiving ground stations are calculated (see section 5.1.1).

- Body fixed frame `IAU_MARS` of Mars:

  This frame is fixed to and does not move with respect to surface features of Mars, but it does move with respect to inertial frames as Mars rotates. The origin is

the center of mass of Mars. The principal plane is the plane of Mars's equator as defined by *Seidelmann et al.* [2001]. This frame is used for computation of the acceleration felt by a spacecraft orbiting Mars from the gravitational field.

- The solar array frames `MEX_SA+Y` and `MEX_SA-Y` of Mars Express (MEX):

  The orientation of the solar panels of MEX with respect to the direction to Sun are needed for a precise computation of the acceleration caused by the solar radiation pressure. This can be realized using the following solar array frames of the left and right solar array `MEX_SA+Y` and `MEX_SA-Y`, respectively. It is defined such as (see figure 2.2)

  - the origin of the frame is located at the geometric center of the yoke,
  - $+Y$ is parallel to the longest side of the solar array, positively oriented from the yoke to the end of the wing,
  - $+Z$ is normal to the solar array plane and the solar cells are facing $+Z$, and
  - $+X$ is defined such that (X, Y, Z) is right handed.

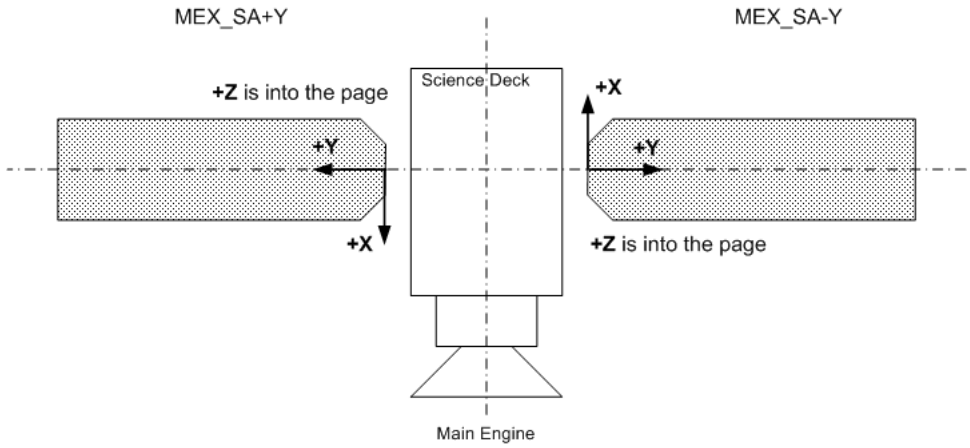

Figure 2.2: *The MEX spacecraft reference system.*

- The solar array frames `ROS_SA+Y` and `ROS_SA-Y` of Rosetta (ROS):

  The orientation of the solar panels of ROS can be computed using the solar array frames. `ROS_SA+Y` and `ROS_SA-Y` defined similar to that of MEX (Fig. 2.2):

  - the origin of the frame is located at the geometric center of the gimbal,
  - $+Y$ axis is parallel to the longest side of the array and array rotation axis, and is positively oriented from the end of the wing toward the gimbal,
  - $+Z$ axis is normal to the solar array plane, the solar cells on the $+Z$ side, and
  - $+X$ axis is defined such that (X, Y, Z) is right handed.

2.3 Transformation from celestial to terrestrial coordinates

Orbit determination from Doppler data requires both celestial reference frames defining a Newtonian-inertial frame, in which the equation of motion can be solved and terrestrial reference frames in which the position of a ground station is defined. The Earth Orientation Parameters (EOPs) establish a connection between these two frames. The EOPs required for a precise transformation between the celestial reference frame and the terrestrial reference frame are provided by *IERS* [2009] and used in form of SPICE kernels. The necessary equations for the transformations are incorporated into the SPICE software package according to *McCarthy and Petit* [2003]. Therefore only a short description of the above mentioned transformation is given below.

Variations in the orientation in space of an Earth-fixed reference frame are driven by variations in the Earth rotation, i.e., in the angular velocity vector of Earth rotation. The rotation of the solid Earth changes as a result of external torques, internal mass redistributions, and the transfer of angular momentum between the solid Earth and the fluid regions. This manifests in variations in direction of Earth-related axes in space (precession and nutation) as well as relative to a terrestrial reference frame (offset of the direction of the rotation axis with the figure axis, polar motion), and also as variation in the angular speed of rotation which translates into variations in the Length of Day (LOD) (see Figure 2.3). Taking into account these effects, the transformation of a position vector $\boldsymbol{r}_{ITRF93}$ in the terrestrial coordinate system `ITRF93` into the celestial coordinate system `J2000` can be carried out via the following transformation rule

$$\boldsymbol{r}_{J2000} = \boldsymbol{\Pi}(t)\,\boldsymbol{N}(t)\,\boldsymbol{\Phi}(t)\,\boldsymbol{P}(t)\,\boldsymbol{r}_{ITRF93}. \tag{2.2}$$

Here, $\boldsymbol{\Pi}(t)$, $\boldsymbol{N}(t)$, $\boldsymbol{\Phi}(t)$ and $\boldsymbol{P}(t)$ are the rotation matrices describing the coordinate changes due to precession, nutation, Earth rotation, and polar motion, respectively. In detail

- **Precession $\boldsymbol{\Pi}(t)$:**

  The orbital plane of the Earth is perturbed from the masses of solar system bodies, this effect is called the planetary precession. The axis of rotation of the Earth is also influenced by the torque which acts on the equatorial wobble from Sun and moon. This is called the lunisolar precession.

- **Nutation $\boldsymbol{N}(t)$:**

  The orientation of the axis of rotation of the Earth is also perturbed by small periodic perturbations that are known as nutation (see Figure 2.3). They are caused by monthly and annual variations of the lunar and solar torques which have been averaged in the consideration of precession.

- **Earth rotation about the Celestial Ephemeris Pole (CEP) $\boldsymbol{\Phi}(t)$:**

  The precession and nutation mentioned above is derived using the CEP, which differs slightly from the instantaneous rotation axis. The rotation about the

CEP axis itself is described by the Greenwich Mean Sidereal Time (GMST) that measures the angle between the mean vernal equinox and the Greenwich Meridian. The GMST can be computed from the difference between UT1 and UTC or UT1 and TAI which is published by *IERS* [2009] and is the instantaneous rate of change of UT1 in seconds, i.e. LOD with respect to a uniform time scale (UTC or TAI).

Similar the Greenwich Apparent Sidereal Time (GAST) measures the hour angle of the true equinox. Both values differ by the nutation in right ascension and are related by the equation of the equinoxes. The transformation matrix $\mathbf{\Phi}(t)$ yields the transformation between the true-of-date coordinate system and a system aligned with the Earth equator and Greenwich meridian from the apparent sidereal time.

- **Polar motion $\boldsymbol{P}(t)$:**

  The Celestial Ephemeris Pole is not fixed with respect to the surface of the Earth and performs a periodic motion around its mean position from which it differs at most 10 m. The polar motion is actually a superposition of mostly two components. Firstly the free precession with a period of about 435 days, the so called Chandler period, and secondly an annual motion that is influenced by seasonal changes of the mass distribution of the Earth caused by water and air flows (Fig. 2.3).

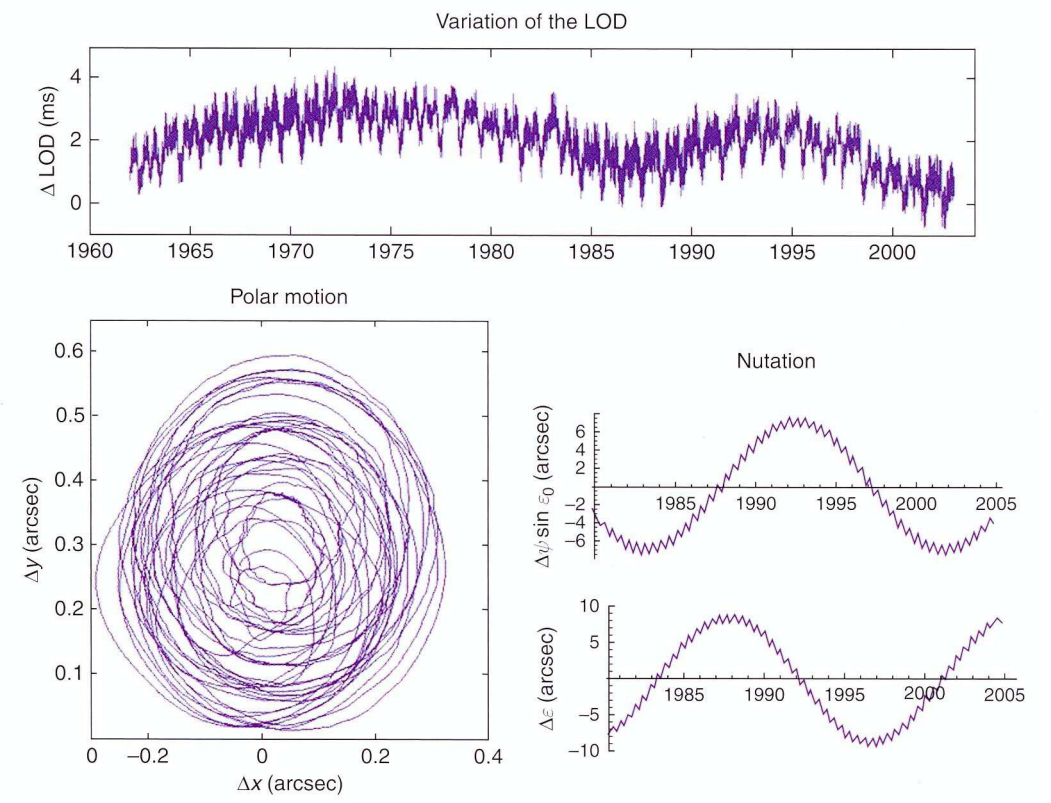

Figure 2.3: *Variations of the Earth Orientation Parameters (EOPs) (Source: Dehant and Mathews [2007]).*

2.4 Integration of the equation of motion

The accurate computation of a satellite's orbit accounting for several forces (see section 3 and 4) can only be obtained by using appropriate numerical methods. A wide range of methods for numerical integration of ordinary differential equations exits. Detailed information is given in *Montenbruck and Gill* [2000], *Vallado* [2001], *Gander* [1985] and *Guthmann* [1994]. In the following the method used in this thesis is described.

The classical Runge-Kutta method, firstly formulated from Carl Runge in 1895 and later from Heun and Kutta improved, is probably the most widely-used method for integration of ordinary differential equations. For the computation of $\boldsymbol{x}_{i+1}$ only the previous computed solution $\boldsymbol{x}_i$ is needed. This is achieved for a step size h_i by an approximation with weighted means. The general Runge-Kutta formula can be written in the form

$$\Phi\left(\boldsymbol{x}, h\right) = \sum_{j=1}^{s} b_j \boldsymbol{k}_j \tag{2.3}$$

with

$$\boldsymbol{k}_j = \boldsymbol{f}\left(\boldsymbol{x} + h \sum_{l=1}^{j-1} a_{jl} \boldsymbol{k}_l\right), \quad 1 \leq j \leq s\,, \tag{2.4}$$

where $\boldsymbol{f}$ describes the equation of motion and s is the stage of the method. Each method is fully described by its coefficients a_{jl}, b_j, which can be written in the following manner

$$\begin{array}{c|cccc} c_1 & 0 & 0 & 0 & 0 \\ c_2 & a_{21} & 0 & 0 & 0 \\ \vdots & \vdots & \ddots & 0 & 0 \\ c_s & a_{s1} & \cdots & a_{s,s-1} & 0 \\ \hline & b_1 & b_2 & \cdots & b_s \end{array}$$

The coefficients are determined such that they satisfy the relations

$$\sum_{i=1}^{s} b_i = 1 \qquad c_j = \sum_{l=1}^{j-1} a_{jl} \quad \text{with} \quad c_1 = 0. \tag{2.5}$$

The accuracy of the method depends on the step size and the computation time on the number of steps to be carried out for computation. Therefore an optimal step size h_i needs to be found for accurate computations with less computation effort.

In order to estimate the error at every step two approximations with the step size h and $\frac{h}{2}$ can be computed and the error according to *Guthmann* [1994] estimated via

$$\delta_i = \frac{\left\| \boldsymbol{x}_{i+1}^{(1)} - \boldsymbol{x}_{i+1}^{(2)} \right\|_\infty}{h_i \left(1 - 2^{-p}\right)} + O\left(h_i^{p+1}\right). \tag{2.6}$$

The disadvantage of this kind of step size control is the large number of function evaluations. A method with stage s has to evaluate the function $\boldsymbol{f}$ on $s + 2s - 1 = 3s - 1$

points and this can lead to an extensive computing time. In order to avoid this disadvantage the embedded methods can be used, which use two approximations $\boldsymbol{x}_{i+1}^{(1)}$ and $\boldsymbol{x}_{i+1}^{(2)}$ of order p and $p+1$, respectively. The essential feature of embedded methods is, that both approximations are obtained by using the same stages $\boldsymbol{k}_j$, thereby decreasing the computational cost for error estimation dramatically. As approximation for the solution at $\boldsymbol{x}_{i+1}$ typically $\boldsymbol{x}_{i+1}^{(1)}$ is used for this method while $\boldsymbol{x}_{i+1}^{(2)}$ is only used for error estimation. The local error for step size control is

$$\delta_i = \frac{\left\| \boldsymbol{x}_{i+1}^{(1)} - \boldsymbol{x}_{i+1}^{(2)} \right\|_\infty}{h_i} + O\left(h_i^{p+1}\right) . \tag{2.7}$$

These embedded methods are called Runge-Kutta-Fehlberg pair with order p and $p+1$, abbreviated *RKFp(p+1)* (*Guthmann* [1994]).

The previously presented methods are using the result of the higher order only for error estimation whereas $\boldsymbol{x}_{i+1}^{(1)}$ is used as approximation of $\boldsymbol{x}\left(t_{i+1}\right)$. *Dormand and Prince* [1981] have developed embedded methods which resolve this disadvantage. As before two approximations $\boldsymbol{x}_{i+1}^{(1)}$, $\boldsymbol{x}_{i+1}^{(2)}$ are computed with methods of order p and q, where usually $q = p+1$. The computation is now continued with $\boldsymbol{x}_{i+1}^{(2)}$ instead of $\boldsymbol{x}_{i+1}^{(1)}$ which leads to a higher accuracy. These method is named *RKp(q)* method. One of the most popular method is the *RK5(4)* method with the tableau defined in table A.3 in the appendix (*Dormand and Prince* [1980]).

The local error estimation via equation (2.7) provides

$$\frac{\boldsymbol{x}_{i+1}^{(1)} - \boldsymbol{x}_{i+1}^{(2)}}{h} = -\frac{71}{57600}\boldsymbol{k}_1 + \frac{71}{16695}\boldsymbol{k}_3 - \frac{71}{1920}\boldsymbol{k}_4 + \frac{17253}{339200}\boldsymbol{k}_5 - \frac{22}{525}\boldsymbol{k}_6 + \frac{1}{40}\boldsymbol{k}_7. \tag{2.8}$$

This method of order 5 and stage 7 needs less computing time than conventional Runge-Kutta methods. It is established in practice and often used in celestial mechanics. In this thesis a numerical integration method is needed which provides a high accuracy at small time steps of one second. *Schwinger* [2001] tested different methods for integrating the equation of motion of a spacecraft orbiting a comet with testing scenarios from *Hull et al.* [1972] and found that the *RK5(4)* method provides also high accuracy by using comparably small step sizes. As the prescribed time step in this work is one second, methods with higher order (see *Dormand and Prince* [1981]) would lose their advantages of high accuracy at large step sizes due to the given small step size of one second.

There are more than the above mentioned methods (see *Montenbruck and Gill* [2000], *Vallado* [2001], *Gander* [1985] and *Guthmann* [1994]), but implementing such a method would go beyond the scope of the thesis. It is shown in section **??** that the selected and implemented integration method *RK5(4)* provides sufficient accuracy and is adequate for solving the equations of motion for Mars Express (MEX) and Rosetta (ROS).

CHAPTER 3

Gravitational forces acting on a spacecraft

The motion of a spacecraft is changed by the gravitational attraction of the central body the spacecraft is orbiting. The central body can be treated as a point mass or if it is irregular shaped and / or has nonuniform mass distribution the deviation from a point mass has also be taken into account for a precise orbit determination. In addition the gravitational attraction of other bodies needs be incorporated into the force model if the gravitational force of these bodies are significant. The relevant mathematical representations and their numerical realization are summarized in this section.

3.1 The two-body equation

In order to change the velocity $\boldsymbol{v}$ of body with constant mass m in an inertial frame a force $\boldsymbol{F}$ is necessary according to Newton's second law

$$\boldsymbol{F} = m\frac{d\boldsymbol{v}}{dt} = m\boldsymbol{a}\,, \tag{3.1}$$

where $\boldsymbol{a}$ is the acceleration due to the force $\boldsymbol{F}$ acting on the body, assuming an ideal inertial reference frame $\boldsymbol{I}$, $\boldsymbol{J}$, $\boldsymbol{K}$ that is fixed in inertial space or has an origin moving with constant velocity. The system of two bodies comprises the central body and a spacecraft with the respective masses m_c and m_{SC}. The bodycentric $\boldsymbol{X}$, $\boldsymbol{Y}$, $\boldsymbol{Z}$-system is displaced from the ideal inertial reference frame $\boldsymbol{I}$, $\boldsymbol{J}$, $\boldsymbol{K}$, but does not rotate or accelerate with respect to $\boldsymbol{I}$, $\boldsymbol{J}$, $\boldsymbol{K}$ (see Figure 3.1). The force acting on the spacecraft in the bodycentric frame can be written according to Newton's law of gravitation as

$$\boldsymbol{F}_g = -Gm_c m_{SC}\frac{\boldsymbol{r}}{|\boldsymbol{r}|^3}\,. \tag{3.2}$$

Here G is the gravitational constant and $\boldsymbol{r}$ the vector from the central body to the spacecraft. This equation is valid only if the central body and the spacecraft can be treated as a point mass and no other force acts on the inertial system. Using the position vector of the central body $\boldsymbol{r}_c$ and the spacecraft $\boldsymbol{r}_{SC}$ with respect to the origin of the $\boldsymbol{I}$, $\boldsymbol{J}$, $\boldsymbol{K}$ reference system a vector from the central body to the spacecraft can be expressed as

$$\boldsymbol{r} = \boldsymbol{r}_{SC} - \boldsymbol{r}_c. \tag{3.3}$$

This equation can be differentiated without considering the derivatives of each axis of the coordinate system due to the fact that the reference system is an inertial system. The acceleration of the spacecraft relative to the center of the central body is then

$$\ddot{\boldsymbol{r}} = \ddot{\boldsymbol{r}}_{SC} - \ddot{\boldsymbol{r}}_c\,. \tag{3.4}$$

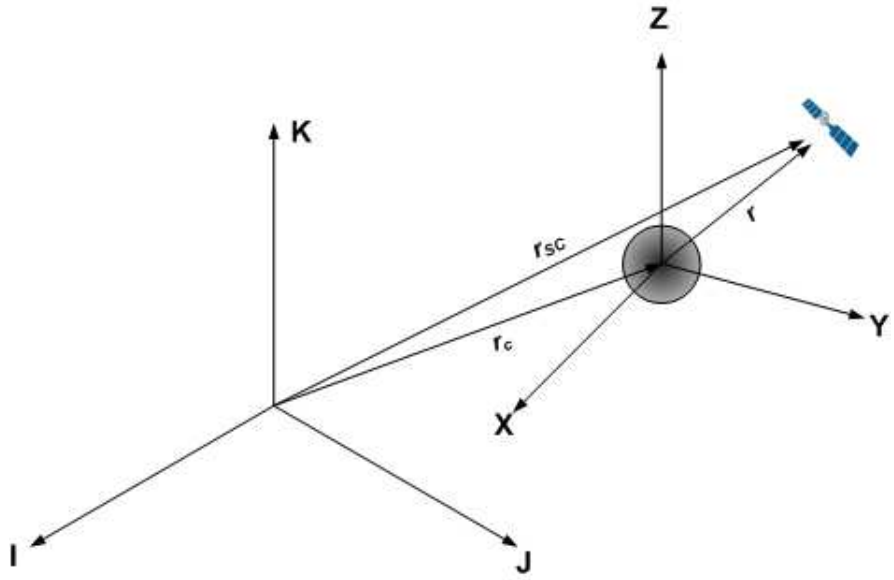

Figure 3.1: *Geometry for two bodies in an inertial reference frame.* $\boldsymbol{I}$, $\boldsymbol{J}$, $\boldsymbol{K}$ *is assumed to be an inertial coordinate system.* $\boldsymbol{X}$, $\boldsymbol{Y}$, $\boldsymbol{Z}$ *is displaced from* $\boldsymbol{I}$, $\boldsymbol{J}$, $\boldsymbol{K}$, *but does not rotate or accelerate with respect to* $\boldsymbol{I}$, $\boldsymbol{J}$, $\boldsymbol{K}$.

Newton's second law and his law of gravitation leads to the following expression for the inertial forces:

$$\boldsymbol{F_{SC}} = m_{SC}\ddot{\boldsymbol{r}}_{SC} = -Gm_c m_{SC}\frac{\boldsymbol{r}}{|\boldsymbol{r}|^3} \tag{3.5}$$

$$\boldsymbol{F_c} = m_c\ddot{\boldsymbol{r}}_c = Gm_c m_{SC}\frac{\boldsymbol{r}}{|\boldsymbol{r}|^3}\,. \tag{3.6}$$

The different signs of the gravitational force on the right side of equations (3.5) and (3.6) originate from the opposite direction of the force of the central body and the force of the spacecraft. The relative acceleration $\ddot{\boldsymbol{r}}$ can now be written by solving for the individual forces and using equation (3.4).

$$\ddot{\boldsymbol{r}} = -G\left(m_c + m_{SC}\right)\frac{\boldsymbol{r}}{|\boldsymbol{r}|^3}\,. \tag{3.7}$$

Assuming that the mass m_{SC} of the spacecraft is very small compared to the mass of the central body m_c and can be neglected, then the two-body equation can be written as

$$\ddot{\boldsymbol{r}} = -Gm_c\frac{\boldsymbol{r}}{|\boldsymbol{r}|^3}\,. \tag{3.8}$$

This is the basic two-body equation which is an idealized approximation and describes the gravitational forces acting on a satellite precisely if the central body can be treated as a point mass. If the central body is orbited also by a moon like the Earth the perturbation of the orbit by the moon has also be taken into account.

3.2 The n-body equation

In the case of a spacecraft orbiting a solar system body the gravitational attraction of the Sun and other bodies must also be taken into account. Therefore an equation which comprises more than one body the so called n-body equation is derived based the two-body equation.

Assuming the same requirements as used in section 3.1 for the two-body equation but introducing a third body as shown in Figure 3.2. The mass of the central body is denoted by m_c, the mass of the third body by m_3, the vector from the central body to the spacecraft by $\boldsymbol{r}$, and the vector from the central body to the third body by $\boldsymbol{r}_3$ (see Figure 3.2). The inertial forces on the spacecraft and the central body are then

$$\boldsymbol{F_{SC}} = m_{SC}\ddot{\boldsymbol{r}}_{SC} = -Gm_c m_{SC}\frac{\boldsymbol{r}}{|\boldsymbol{r}|^3} - Gm_3 m_{SC}\frac{\boldsymbol{r}-\boldsymbol{r}_3}{|\boldsymbol{r}-\boldsymbol{r}_3|^3} \tag{3.9}$$

$$\boldsymbol{F_c} = m_c\ddot{\boldsymbol{r}}_c = Gm_c m_{SC}\frac{\boldsymbol{r}}{|\boldsymbol{r}|^3} + Gm_c m_3\frac{\boldsymbol{r}_3}{|\boldsymbol{r}_3|^3}\,. \tag{3.10}$$

The acceleration felt by the spacecraft relative to the mass center of the central body is according to equation (3.3)

$$\ddot{\boldsymbol{r}} = -Gm_c\frac{\boldsymbol{r}}{|\boldsymbol{r}|^3} - Gm_3\frac{\boldsymbol{r}-\boldsymbol{r}_3}{|\boldsymbol{r}-\boldsymbol{r}_3|^3} + Gm_{SC}\frac{\boldsymbol{r}}{|\boldsymbol{r}|^3} + Gm_3\frac{\boldsymbol{r}_3}{|\boldsymbol{r}_3|^3}\,, \tag{3.11}$$

Reordering the terms and the assumption that the mass m_{SC} of the spacecraft is negligible produces

$$\ddot{\boldsymbol{r}}_3 = -Gm_c\frac{\boldsymbol{r}}{|\boldsymbol{r}|^3} - Gm_3\left(\frac{\boldsymbol{r}-\boldsymbol{r}_3}{|\boldsymbol{r}-\boldsymbol{r}_3|^3} + \frac{\boldsymbol{r}_3}{|\boldsymbol{r}_3|^3}\right)\,. \tag{3.12}$$

The first term the two-body acceleration of the spacecraft due to the central body. The left-hand term in the bracket is called the direct effect and represents the acceleration of the third body directly on the satellite. The right-hand term is the acceleration of the third body on the central body and is named consequentially the indirect term. Expanding equation (3.12) to n bodies and leads to the n-body equation

$$\ddot{\boldsymbol{r}} = -Gm_c\frac{\boldsymbol{r}}{|\boldsymbol{r}|^3} - \sum_{i=1}^{n} Gm_i\left(\frac{\boldsymbol{r}-\boldsymbol{r}_i}{|\boldsymbol{r}-\boldsymbol{r}_i|^3} + \frac{\boldsymbol{r}_i}{|\boldsymbol{r}_i|^3}\right)\,. \tag{3.13}$$

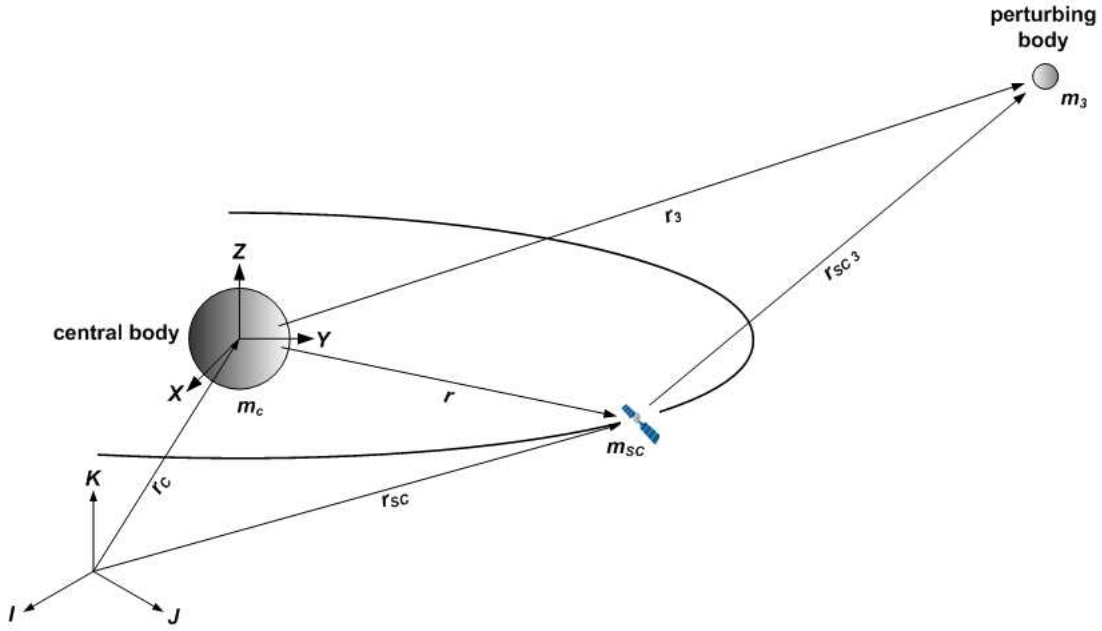

Figure 3.2: *Geometry of the three-body problem in an inertial reference frame* $\boldsymbol{I}$, $\boldsymbol{J}$, $\boldsymbol{K}$.

3.3 Sphere of influence

In equation (3.13) the central body represents the body with the highest gravitational attraction on the spacecraft. Sometimes it is not clear which is the body with the highest gravitational attraction regarding the mass of the bodies and distance from each other. But wrong selection of the central body would lead to inaccurate orbit determination.

This problem can be solved with the concept of the sphere of influence. The sphere of influence for a central body is an imaginary sphere within the gravity of the object is primarily responsible for all orbital motion. Outside this sphere, other bodies influence most of the spacecrafts motion.

Assuming three bodies with masses m_1, m_2 and m_3 (Fig. 3.3), m_1 is the central body, m_2 the spacecraft, and m_3 the perturbing body, the equation of motion can be written according to equation (3.13)

$$\ddot{\boldsymbol{r}}_{12} + G\left(m_1 + m_2\right)\frac{\boldsymbol{r}_{12}}{r_{12}^3} = -Gm_3\left(\frac{\boldsymbol{r}_{13}}{r_{13}^3} + \frac{\boldsymbol{r}_{32}}{r_{32}^3}\right) . \tag{3.14}$$

If the central body is m_3 and m_1 the perturbing body the equation of motion is accordingly

$$\ddot{\boldsymbol{r}}_{32} + G\left(m_3 + m_2\right)\frac{\boldsymbol{r}_{32}}{r_{32}^3} = -Gm_1\left(\frac{\boldsymbol{r}_{12}}{r_{12}^3} - \frac{\boldsymbol{r}_{13}}{r_{13}^3}\right) . \tag{3.15}$$

From this equations it can be distinguished, by the ratio of the disturbing force (right hand side of the equations) to the corresponding central attraction (left hand side), which of the equations has to be used. Whichever provides the smaller ratio is the one to be preferred.

The surface boundary over which these two ratios are equal is almost spherical if $r_{12} \ll r_{13}$. Equating both ratios and assuming that $m_3 \ll m_1$ and $m_1 \gg m_2$ the sphere of influence about m_1 is approximately

$$\frac{r_{12}}{r_{13}} = \left(\frac{m_1}{m_3}\right)^{\frac{2}{5}} . \tag{3.16}$$

This equation describes a sphere about m_1 on the boundary of which the ratio of disturbing to primary accelerations is the same for both equations (3.14) and (3.15). Inside the sphere the motion of m_2 relative to m_1 should be computed and outside m_3 should be treated as the central body. A table of the sphere of influence for the planets with respect to the Sun can be found in *Battin* [1987], page 397 or in *Häusler* [2008*c*].

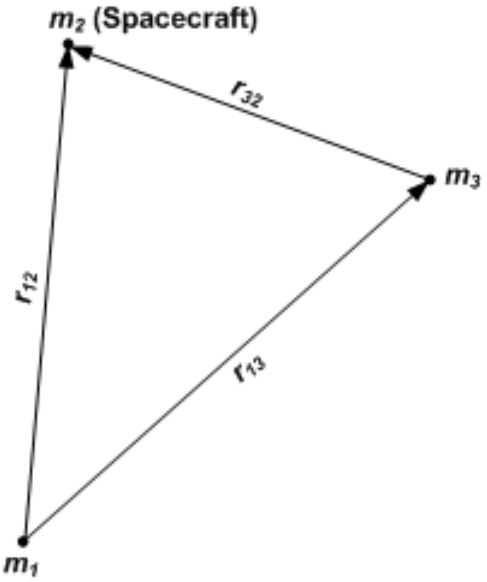

Figure 3.3: *Sphere of influence (Source: Häusler [2008c], changed).*

3.4 The gravity potential of a body

In the previous sections the equation of motion for a satellite orbiting a central body was developed based on the assumption that all bodies can be treated as point masses. However this is in most cases not true for practical purposes. Mars for instance consists of large volcanoes but also of valleys and this leads to a gravity field strongly deviating from a point mass representation. In the following the gravity potential of a body with non-spherical shape and a nonuniform density distribution is derived. In addition, a numerical implementation is developed with which the acceleration felt by satellite orbiting around such a body can be computed precisely.

The acceleration of a body according to equation (3.8) can also be written using a potential U in the form

$$\ddot{\boldsymbol{r}} = -\text{grad}\,(U) \qquad \text{with} \qquad U = Gm_c\frac{1}{r}. \tag{3.17}$$

The mass of a body can be expressed by the sum of a large but finite number of very small mass elements dm. The summation of each mass element over the entire body results in the potential of a body with arbitrary shape and density distribution

$$U(\boldsymbol{r}) = G\iiint\limits_{Vol}\frac{\rho(\boldsymbol{s})}{|\boldsymbol{r}-\boldsymbol{s}|}dV\,, \tag{3.18}$$

where $\boldsymbol{r}$ is the position vector of the point in which the potential is determined and $\boldsymbol{s}$ the position vector of the infinitesimal mass dm of the body (Fig. 3.4), which are expressed using the individual density and volume of the specific mass element

$$dm = \rho(\boldsymbol{s})dV \tag{3.19}$$

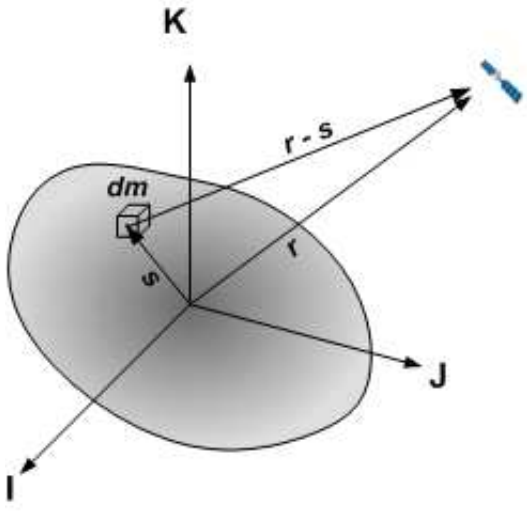

Figure 3.4: *Contribution of a small mass element to the gravity potential of a body.*

3.4.0.1 Expansion of the gravity potential in spherical harmonics

In order to determine the gravity potential of an irregular shaped body using equation (3.18) the inverse of the distance $|\boldsymbol{r}-\boldsymbol{s}|$ can be expanded in a series of Legendre polynomials. For this purpose the origin of the coordinate system has to align with the center of mass and a reference radius is selected which fulfills the condition $\bar{R} := \max\{|\boldsymbol{s}| \; | \boldsymbol{s} \in Vol\}$. $\bar{R}$ describes a sphere enclosing the body and $\boldsymbol{r}$ lies outside of the body if $|\boldsymbol{r}| > \bar{R}$ for all points, so that

$$\frac{1}{|\boldsymbol{r}-\boldsymbol{s}|} = \frac{1}{r}\sum_{n=0}^{\infty}\left(\frac{s}{r}\right)^n \mathrm{P}_n(\cos\gamma) \quad \text{with} \quad \cos\gamma = \frac{\boldsymbol{r}\cdot\boldsymbol{s}}{r\,s}\,, \tag{3.20}$$

where γ is the angle between $\boldsymbol{r}$ and $\boldsymbol{s}$, and

$$\mathrm{P}_n(x) = \frac{1}{2^n n!}\frac{d^n}{dx^n}\left(x^2-1\right)^n \tag{3.21}$$

is the Legendre polynomial or zonal spherical harmonics of degree n. Introducing spherical coordinates, i.e. radius r, latitude ϕ and longitude λ of the point $\boldsymbol{r}$ and analogue r', ϕ', λ' of $\boldsymbol{s}$, the addition theorem of Legendre polynomials (*Kautzleben* [1965])

$$\mathrm{P}_n(\cos\gamma) = \sum_{m=0}^{n}(2-\delta_{0,m})\frac{(n-m)!}{(n+m)!}\,\mathrm{P}_{n,\,m}(\cos\phi)\,\mathrm{P}_{n,\,m}(\cos\phi')\,\cos m(\lambda-\lambda') \tag{3.22}$$

can be used, where $\delta_{0,m}$ is the Kronecker delta symbol and $\mathrm{P}_{n,\,m}(x)$ are the associated Legendre polynomials of degree n and order m which are defined by

$$\mathrm{P}_{n,\,m}(x) = (1-x^2)^{(m/2)}\,\frac{d^m\,\mathrm{P}_n(x)}{d\,x^m}. \tag{3.23}$$

This formulation is inefficient for practical computation. A more efficient way to calculate these functions can be accomplished by recursion. This method is described in detail in *Press et al.* [1986] or *Vallado* [2001].

Inserting the associated Legendre polynomial and equation (3.20) into equation (3.18) the gravity potential of non-spherical body can be written as

$$U = \frac{Gm_c}{r}\sum_{n=0}^{\infty}\sum_{m=0}^{n}\left(\frac{\bar{R}}{r}\right)^n \mathrm{P}_{n,\,m}(\cos\phi)\,(\mathrm{C}_{n,\,m}\cos m\lambda + \mathrm{S}_{n,\,m}\sin m\lambda) \tag{3.24}$$

$$= \frac{Gm_c}{r}\sum_{n=0}^{\infty}\sum_{m=0}^{n}\left(\frac{\bar{R}}{r}\right)^n \left(\mathrm{C}_n^m\,(\phi,\,\lambda)\,\mathrm{C}_{n,\,m} + \mathrm{S}_n^m\,(\phi,\,\lambda)\,\mathrm{S}_{n,\,m}\right)\,, \tag{3.25}$$

where the $C_{n,\,m}$ and $S_{n,\,m}$ are the gravitational coefficients defined as

$$C_{n,\,m} = \frac{2-\delta_{0,m}}{m_c}\frac{(n-m)!}{(n+m)!}\iiint\limits_{Vol}\left(\frac{s}{\overline{R}}\right)^n P_{n,\,m}(\cos\phi')\cos(m\lambda')\rho\,(r',\ \phi',\ \lambda')\ dV \quad (3.26a)$$

$$S_{n,\,m} = \frac{2-\delta_{0,m}}{m_c}\frac{(n-m)!}{(n+m)!}\iiint\limits_{Vol}\left(\frac{s}{\overline{R}}\right)^n P_{n,\,m}(\cos\phi')\sin(m\lambda')\rho\,(r',\ \phi',\ \lambda')\ dV\,. \quad (3.26b)$$

These coefficients describe the dependence of internal mass distributions within the body and are used for precise orbit determination around a non-spherical body.

The $C_n^m(\phi,\,\lambda)$ and $S_n^m(\phi,\,\lambda)$ in equation (3.25) are called spherical harmonics and determine lines on a sphere by the indices n and m along which the functions vanish. The spherical harmonics can be divided into three different types (see Figure 3.5): zonal, sectorial and tesseral harmonics.

Zonal harmonics are characterized by the fact that the index m equals zero. Therefore the potential is no longer depending on the longitude λ. The potential is symmetric along the pole axis. The sphere is divided in $n+1$ bands of latitude, in which the potential is alternately increasing (+) and decreasing (-), i.e. every root of the zonal harmonics indicates a transition between negative and positive values (Fig. 3.5(a)).

Sectorial harmonics are defined by $n = m$. and displaying bands of longitude on the sphere as it can be seen in figure 3.5(b). The Legendre polynomials $P_{n,\,n}$ are only zero at the poles in this case. In addition the term $(\sin(n\lambda) + \cos(n\lambda))$ vanishes also for $2n$ different values of λ. Therefore, the line along which the spherical harmonics $C_n^m(\phi,\,\lambda)$ and $S_n^m(\phi,\,\lambda)$ equal zero indicates meridians which divide the sphere in $2n$ sectors. Every sector indicates n positive (+) and n negative mass concentrations.

If $n \neq 0$ and $m \neq 0$ then specific regions of the body are represented and these functions are called *tesseral harmonics*. The sphere is divided into the form of a checkerboard as shown in Figure 3.5(c) (*Vallado* [2001]).

3.4.1 Gravitational coefficients

The gravitational coefficients from equations (3.26a) and (3.26b) serve as weighting factors in the expansion of the potential of a body with nonuniform mass distribution. As the origin of the coordinate system is aligned with the center of mass, some of the low-degree and order coefficients can be simplified in the following form.

- If $m = 0$ and $n = 0$ then from equation (3.26a) it can be derived that

$$C_{0,\,0} = \frac{1}{m_c}\iiint\limits_{\mathrm{Vol}}\rho\,(\boldsymbol{s})\,dV = 1. \quad (3.27)$$

- If $m = 0$ then the term $\sin(m\lambda')$ equals zero and therefore

$$S_{n,\,0} = 0 \qquad \text{for all } n. \quad (3.28)$$

- The following gravity coefficients are vanishing.

$$\begin{aligned} \mathrm{C}_{1,\,0} &= \frac{1}{m_c \bar{R}} \iiint\limits_{\mathrm{Vol}} s \cos\theta' \rho(\boldsymbol{s}) dV \qquad (3.29) \\ &= \frac{1}{m_c \bar{R}} \iiint\limits_{\mathrm{Vol}} z' \rho(\boldsymbol{s}) dV \\ &= \frac{\bar{z}}{\bar{R}} \\ \mathrm{C}_{1,\,1} &= \frac{\bar{x}}{\bar{R}} \qquad (3.30) \\ \mathrm{S}_{1,\,1} &= \frac{\bar{y}}{\bar{R}}, \qquad (3.31) \end{aligned}$$

  where $\bar{x}$, $\bar{y}$, $\bar{z}$ are the coordinates of the center of mass defined by

$$\bar{\boldsymbol{r}} = \begin{pmatrix} \bar{x} \\ \bar{y} \\ \bar{z} \end{pmatrix} \frac{1}{m_c} \int \boldsymbol{s} \rho(\boldsymbol{s}) \, d^3\boldsymbol{s}. \qquad (3.32)$$

- If the axis of the coordinate system are selected in the way that they are aligned with the main axis of inertia, i.e. the off-diagonal elements of the inertia tensor I_{xy}, I_{yz} and I_{xz} vanish then

$$\begin{aligned} \mathrm{C}_{2,\,1} &= \frac{2}{6 m_c \bar{R}^2} \iiint\limits_{\mathrm{Vol}} 3 \cos\theta' \sin\theta' \cos\phi' \rho(\boldsymbol{s}) dV \qquad (3.33) \\ &= \frac{1}{m_c \bar{R}^2} \iiint\limits_{\mathrm{Vol}} xz \, \rho(\boldsymbol{s}) dV \\ &= -\frac{I_{xz}}{m_c \bar{R}^2} = 0 \end{aligned}$$

  and accordingly:

$$\begin{aligned} \mathrm{S}_{2,\,1} &= -\frac{I_{yz}}{M \bar{R}^2} = 0 \qquad (3.34) \\ \mathrm{S}_{2,\,2} &= -\frac{I_{xy}}{2 M \bar{R}^2} = 0\,. \qquad (3.35) \end{aligned}$$

Therefore the lowest order gravitational coefficients, which are not vanishing, are $\mathrm{C}_{2,\,0}$ and $\mathrm{C}_{2,\,2}$, if the coordinate system is well selected. The coefficient $\mathrm{C}_{2,\,0}$ represents the flattening of the body, i.e. the difference between the polar and the equatorial diameter and is for example the largest coefficient for the Earth's gravity potential, being three orders of magnitude larger than $\mathrm{C}_{3,\,0}$, which accounts for bulb-like shape of the Earth.

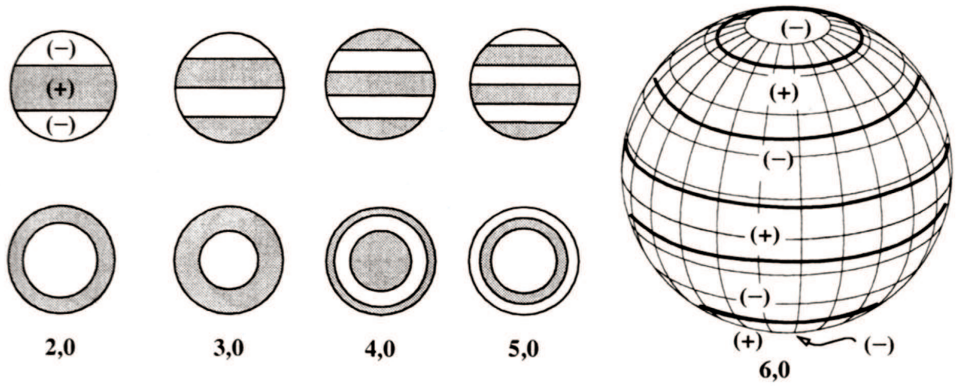

(a) Zonal harmonics

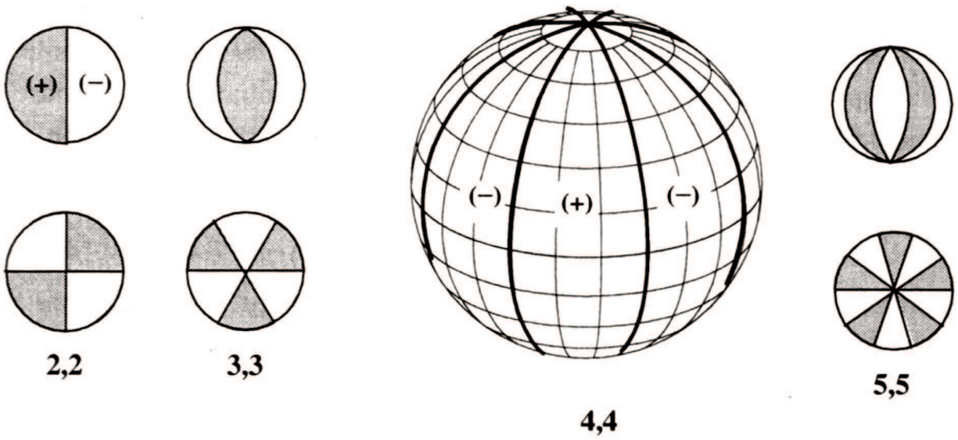

(b) Sectorial harmonics

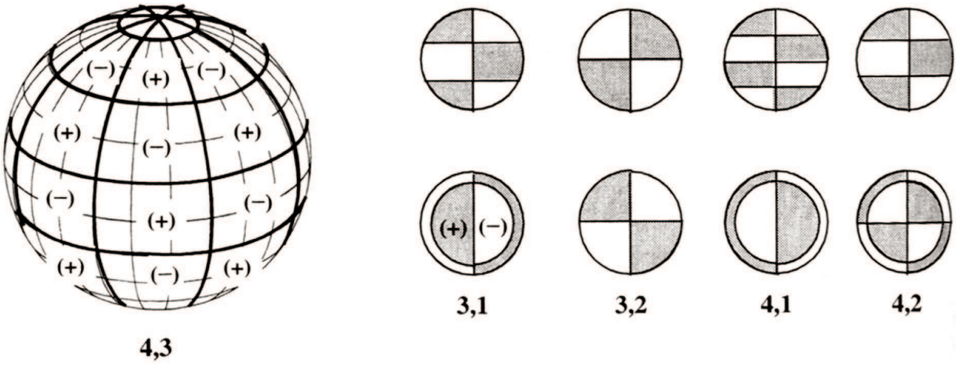

(c) Tesseral harmonics

Figure 3.5: *Spherical harmonics (Source: Vallado [2001], changed)*

3.4.2 Normalization

The gravitational coefficients may differ over a range of ten or more orders of magnitude. Therefore, normalized coefficients are used in practice which are much more uniform and provide higher accuracy for gravity potential computation. The normalization is defined as

$$\Pi_{n,\,m} = \sqrt{\frac{(n+m)!}{(2-\delta_{0,m})\,(n-m)!\,(2n+1)}}\,. \tag{3.36}$$

Thus the normalized coefficients of the expansion are

$$\begin{Bmatrix} \overline{\mathrm{C}}_{n,\,m} \\ \overline{\mathrm{S}}_{n,\,m} \end{Bmatrix} = \Pi_{n,\,m} \begin{Bmatrix} \mathrm{C}_{n,\,m} \\ \mathrm{S}_{n,\,m} \end{Bmatrix}. \tag{3.37}$$

And the normalized associated Legendre polynomials are

$$\overline{\mathrm{P}}_{n,\,m} = \frac{\mathrm{P}_{n,\,m}}{\Pi_{n,\,m}}. \tag{3.38}$$

Obviously, the product of the unnormalized Legendre polynomials and the unnormalized coefficients is equal to the product of the normalized Legendre polynomials and the normalized coefficients, i.e.

$$\overline{\mathrm{C}}_{n,\,m}\overline{\mathrm{P}}_{n,\,m} = \mathrm{C}_{n,\,m}\mathrm{P}_{n,\,m} \quad \text{and} \quad \overline{\mathrm{S}}_{n,\,m}\overline{\mathrm{P}}_{n,\,m} = \mathrm{S}_{n,\,m}\mathrm{P}_{n,\,m} \tag{3.39}$$

Equation (3.36) defines the normalization coefficients most commonly used in geophysical science. Most published gravitational coefficients are based on this normalization, although other definitions of normalization factors do exist (see *Kautzleben* [1965]).

3.4.3 Time varying gravitational coefficients

In the previous section the central body was treated as a point mass or as a rigid body with an irregular shape and therefore a nonuniform gravity potential. However, no solar system body is perfectly rigid and thus subjected to time varying deformations due to tidal forces.

These forces are caused by the difference in gravitational attraction and centrifugal forces, i.e. the difference in the attraction at points inside and outside the central body experiencing by the gravitational attraction of an orbiting body. The impact of the relative small difference forces is significant. The major part of the attraction is compensated by the centrifugal force arising by orbiting around the barycenter of the two bodies. But the centrifugal force has the same amplitude and direction at all locations because all points of the central body are describing congruent orbits. Therefore it only compensates the gravitational force at the center of mass of the

central body and all other points experience a differential force, which is called tidal force (*Kertz* [1995], *Agnew* [2007]).

In the case of the Earth, the tidal forces of the Moon and the Sun acting on the Earth result in a small time varying deformation of the solid body of the Earth. The oceans also respond to the gravitational attraction of the Moon and the Sun and the effect is called ocean tides. Therefore the Earth's gravity field is not constant in time but shows small periodic changes. These small variations in the gravity field also effect the motion of a spacecraft. In the case of Mars only the gravity field of the Sun distorts the shape of Mars.

The change in the gravity coefficients of a central body due to solid tides of can be written according to *McCarthy and Petit* [2003]:

$$\begin{Bmatrix} \Delta \mathrm{C}_{n,\,m} \\ \Delta \mathrm{S}_{n,\,m} \end{Bmatrix} = \frac{k_{n,\,m}}{2n+1} \sum_{i=1}^{l} \frac{m_j}{m_c} \left(\frac{\overline{R}}{r_i} \right)^{n+1} \overline{\mathrm{P}}_{n,\,m} \left(\sin \left(\phi_i \right) \right) \begin{Bmatrix} \cos \left(m\lambda_i \right) \\ \sin \left(m\lambda_i \right) \end{Bmatrix} \tag{3.40}$$

where $k_{n,\,m}$ are the nominal Love numbers of degree n and order m, m_i is the mass of the disturbing body like moon or sun in the case of the Earth, m_c the mass of the central body, $\overline{R}$ the equatorial radius of the central body, r_i the distance from the center of the central body to the disturbing one, ϕ_i is the body-fixed latitude and λ the body-fixed longitude of the disturbing body and $\overline{\mathrm{P}}_{n,\,m}$ the normalized associated Legendre polynomials. The variation of the largest gravity coefficients $\overline{\mathrm{C}}_{2,\,0}$ and $\overline{\mathrm{C}}_{3,\,0}$ can than be computed via

$$\Delta \overline{\mathrm{C}}_{2,\,0} = \frac{k_{2,\,0}}{2\sqrt{5}} \sum_{i=1}^{l} \frac{m_j}{m_c} \left(\frac{\overline{R}}{r_i} \right)^{3} \left(3 \sin \left(\phi_i \right)^2 - 1 \right) \tag{3.41}$$

$$\Delta \overline{\mathrm{C}}_{3,\,0} = \frac{k_{3,\,0}}{2\sqrt{7}} \sum_{i=1}^{l} \frac{m_j}{m_c} \left(\frac{\overline{R}}{r_i} \right)^{4} \left(5 \sin \left(\phi_i \right)^3 - 3 \sin \left(\phi_i \right) \right) \tag{3.42}$$

Another effect resulting from the tidal deformations is a change in position of a ground station located on the surface of the Earth. Detailed information on this effect will be given in section 5.1.1.

3.5 Numerical computation of the gravitational acceleration of an irregular shaped body

Computing the gradient of the gravity potential of an irregular shaped body according to equation (3.24) is quite time consuming. Therefore an optimized algorithm is useful to save time in repetitive calculation. *Cunningham* [1970] formulated a recursion algorithm and *Montenbruck and Gill* [2000] adopted it (a detailed description can be found in appendix A.4). This algorithm is suitable for a direct computation of the acceleration felt by spacecraft in a body-fixed frame. It uses unnormalized gravitational coefficients

$\mathrm{C}_{n,\,m}$ and $\mathrm{S}_{n,\,m}$, which makes the algorithm numerical inaccurate due to the small size of the unnormalized gravitational coefficients of high degree n and order m. This algorithm is modified in this thesis for use with normalized gravitational coefficients $\overline{\mathrm{C}}_{n,\,m}$ and $\overline{\mathrm{S}}_{n,\,m}$ ensuring high accuracy of the computed acceleration. The modification of the algorithm is explained in the following.

The gravity potential of a irregular shaped body using normalized gravitational coefficients $\overline{\mathrm{C}}_{n,\,m}$ and $\overline{\mathrm{S}}_{n,\,m}$ is analogue defined to the definition in *Montenbruck and Gill* [2000]

$$U = \frac{GM}{\bar{R}} \sum_{n=0}^{\infty} \sum_{m=0}^{n} \left(\overline{\mathrm{C}}_{n,\,m} \overline{\mathrm{V}}_{n,\,m} + \overline{\mathrm{S}}_{n,\,m} \overline{\mathrm{W}}_{n,\,m} \right) , \tag{3.43}$$

with the normalized recursion coefficients

$$\overline{\mathrm{V}}_{n,\,m} = \left(\frac{\bar{R}}{r} \right)^{n+1} \overline{\mathrm{P}}_{n,\,m} \left(\sin \phi \right) \cos \left(m\lambda \right) \tag{3.44a}$$

$$\overline{\mathrm{W}}_{n,\,m} = \left(\frac{\bar{R}}{r} \right)^{n+1} \overline{\mathrm{P}}_{n,\,m} \left(\sin \phi \right) \sin \left(m\lambda \right) , \tag{3.44b}$$

and the radius r, the latitude ϕ, the longitude λ of the point $\boldsymbol{r}$, and the reference radius $\overline{\mathrm{R}}$ as defined in section 3.4.0.1.

The relation between normalized and unnormalized gravity coefficients and Legendre polynomials is

$$\overline{\mathrm{C}}_{n,\,m}\, \overline{\mathrm{P}}_{n,\,m} = \mathrm{C}_{n,\,m}\, \mathrm{P}_{n,\,m} \qquad \text{and} \qquad \overline{\mathrm{S}}_{n,\,m}\, \overline{\mathrm{P}}_{n,\,m} = \mathrm{S}_{n,\,m}\, \mathrm{P}_{n,\,m} . \tag{3.45}$$

In order to normalize the Legendre polynomials the following normalization factor (see section 3.4.2) is used

$$\Pi_{n,\,m} = \sqrt{\frac{(2 - \delta_{0,m})\,(n-m)!\,(2n+1)}{(n+m)!}} . \tag{3.46}$$

In recursion algorithms the current result is computed from previous ones like

$$\mathrm{P}_{n,\,m} = \mathrm{P}_{n-i,\,m-j}\ (...) \qquad \text{with } i,\, j \in \mathbb{N} . \tag{3.47}$$

Therefore, the normalized recurrence coefficients can be computed based on the algorithm in *Montenbruck and Gill* [2000] using a compensation factor $\mathrm{X}_{n,\,m}^{(i,\,j)}$ which satisfies the following relation using the normalization factor defined in equation (3.36) and the relation between normalized and unnormalized gravitational coefficients and Legendre polynomials from equation (3.39)

$$\Pi_{n,\,m}\, \mathrm{P}_{n,\,m} = \mathrm{X}_{n,\,m}^{(i,\,j)}\, \Pi_{n+i,\,m+j}\, \mathrm{P}_{n+i,\,m+j}\,(...) . \tag{3.48}$$

This yields for the compensation factor

$$\mathrm{X}_{n,\,m}^{(i,\,j)} = \frac{\Pi_{n,\,m}}{\Pi_{n+i,\,m+j}}\,. \tag{3.49}$$

Initial conditions for the recurrence coefficients are according to *Montenbruck and Gill* [2000]

$$\overline{\mathrm{V}}_{0,\,0} = \frac{\overline{\mathrm{R}}}{r} \quad \text{and} \quad \overline{\mathrm{W}}_{0,\,0} = 0 \tag{3.50}$$

In order to compute the recurrence coefficients $\overline{\mathrm{V}}_{m,\,n}$ and $\overline{\mathrm{W}}_{n,\,m}$ the following compensation factors are needed.

$$\mathrm{X}_{m,\,m}^{(-1,\,-1)} \overset{m\geq 0}{=} \frac{\Pi_{m,\,m}}{\Pi_{m-1,\,m-1}} = \frac{1}{2m-1}\sqrt{\frac{(2m+1)}{(2-\delta_{0,m-1})\,m}} \tag{3.51}$$

$$\mathrm{X}_{n,\,m}^{(-1,\,0)} = \frac{\Pi_{n,\,m}}{\Pi_{n-1,\,m}} = \sqrt{\frac{(2n+1)\,(n-m)}{(n+m)\,(2n-1)}} \tag{3.52}$$

$$\mathrm{X}_{n,\,m}^{(-2,\,0)} = \frac{\Pi_{n,\,m}}{\Pi_{n-2,\,m}} = \sqrt{\frac{(2n+1)\,(n-m)\,(n-m-1)}{(n+m)\,(n+m-1)\,(2n-3)}} \tag{3.53}$$

With these compensation factors $\mathrm{X}_{n,\,m}^{(i,\,j)}$ the normalized recurrence coefficients are

$$\begin{aligned}\overline{\mathrm{V}}_{m,\,m} &\overset{m\geq 0}{=} \frac{\overline{\mathrm{R}}}{r^2}\,\mathrm{X}_{m,\,m}^{(-1,\,-1)}\,(2m-1)\left(x\,\overline{\mathrm{V}}_{m-1,\,m-1} - y\,\overline{\mathrm{W}}_{m-1,\,m-1}\right)\\ &= \frac{\overline{\mathrm{R}}}{r^2}\sqrt{\frac{2m+1}{(2-\delta_{0,m-1})\,m}}\left(x\,\overline{\mathrm{V}}_{m-1,\,m-1} - y\,\overline{\mathrm{W}}_{m-1,\,m-1}\right)\end{aligned} \tag{3.54a}$$

$$\begin{aligned}\overline{\mathrm{W}}_{m,\,m} &\overset{m\geq 0}{=} \frac{\overline{\mathrm{R}}}{r^2}\,\mathrm{X}_{m,\,m}^{(-1,\,-1)}\,(2m-1)\left(x\,\overline{\mathrm{W}}_{m-1,\,m-1} + y\,\overline{\mathrm{V}}_{m-1,\,m-1}\right)\\ &= \frac{\overline{\mathrm{R}}}{r^2}\sqrt{\frac{2m+1}{(2-\delta_{0,m-1})\,m}}\left(x\,\overline{\mathrm{W}}_{m-1,\,m-1} + y\,\overline{\mathrm{V}}_{m-1,\,m-1}\right)\end{aligned} \tag{3.54b}$$

$$\begin{aligned}\overline{\mathrm{V}}_{n,\,m} &= \frac{\overline{\mathrm{R}}}{r^2}\,\frac{1}{(n-m)}\Big(\mathrm{X}_{n,\,m}^{(-1,\,0)}\,(2n-1)\,z\,\overline{\mathrm{V}}_{n-1,\,m}\\ &\qquad - \mathrm{X}_{n,\,m}^{(-2,\,0)}\,(n+m-1)\,\overline{\mathrm{R}}\,\overline{\mathrm{V}}_{n-2,\,m}\Big)\\ &= \frac{\overline{\mathrm{R}}}{r^2}\sqrt{\frac{2n+1}{(n+m)\,(n-m)}}\Bigg(\sqrt{2n-1}z\,\overline{\mathrm{V}}_{n-1,\,m}\\ &\qquad - \sqrt{\frac{(n+m-1)\,(n-m-1)}{2n-3}}\overline{\mathrm{R}}\,\overline{\mathrm{V}}_{n-2,\,m}\Bigg)\end{aligned} \tag{3.54c}$$

$$\begin{aligned}\overline{\mathrm{W}}_{n,\,m} &= \frac{\overline{\mathrm{R}}}{r^2}\,\frac{1}{(n-m)}\Big(\mathrm{X}^{(-1,\,0)}_{n,\,m}\,(2n-1)\,z\,\overline{\mathrm{W}}_{n-1,\,m} \\ &\quad - \mathrm{X}^{(-2,\,0)}_{n,\,m}\,(n+m-1)\,\overline{\mathrm{R}}\,\overline{\mathrm{W}}_{n-2,\,m}\Big) \\ &= \frac{\overline{\mathrm{R}}}{r^2}\,\sqrt{\frac{2n+1}{(n+m)\,(n-m)}}\Bigg(\sqrt{2n-1}z\,\overline{\mathrm{W}}_{n-1,\,m} \\ &\quad - \sqrt{\frac{(n+m-1)\,(n-m-1)}{2n-3}}\overline{\mathrm{R}}\,\overline{\mathrm{W}}_{n-2,\,m}\Bigg) \end{aligned} \tag{3.54d}$$

In order to compute the acceleration from normalized gravitational coefficients a compensation factor must be implemented as a moderator between the normalized gravity coefficients $\overline{\mathrm{C}}_{n,\,m}$, $\overline{\mathrm{S}}_{n,\,m}$ and the normalized recurrence coefficients $\overline{\mathrm{V}}_{n,\,m}$, $\overline{\mathrm{W}}_{n,\,m}$, because they are multiplied with different degree and order. Therefore the following condition has to be complied with

$$\begin{aligned}\mathrm{C}_{n,\,m}\,\mathrm{P}_{n+i,\,m+j} &= \frac{1}{\Pi_{n,\,m}}\,\mathrm{C}_{n,\,m}\,\mathrm{X}^{(i,\,j)}_{n,\,m}\,\Pi_{n+i,\,m+j}\,\mathrm{P}_{n+i,\,m+j} \\ &= \overline{\mathrm{C}}_{n,\,m}\,\mathrm{X}^{(i,\,j)}_{n,\,m}\,\overline{\mathrm{P}}_{n+i,\,m+j} \end{aligned} \tag{3.55}$$

Hence, the compensation factor for the acceleration is equally defined as for the recursion coefficients in equation (3.49).

The specific compensation factors necessary for further computations can be derived as follows

$$\mathrm{X}^{(1,\,1)}_{n,\,0} = \frac{\Pi_{n,\,0}}{\Pi_{n+1,\,1}} = \sqrt{\frac{(2n+1)\,(n+1)\,(n+2)}{2\,(2n+3)}} \tag{3.56}$$

$$\mathrm{X}^{(1,\,0)}_{n,\,0} = \frac{\Pi_{n,\,0}}{\Pi_{n+1,\,0}} = \sqrt{\frac{2n+1}{2n+3}} \tag{3.57}$$

$$\mathrm{X}^{(1,\,1)}_{n,\,m} \overset{m\geq 0}{=} \frac{\Pi_{n,\,m}}{\Pi_{n+1,\,m+1}} = \sqrt{\frac{(2n+1)\,(n+m+2)\,(n+m+1)}{2n+3}} \tag{3.58}$$

$$\mathrm{X}^{(1,\,-1)}_{n,\,m} \overset{m\geq 0}{=} \frac{\Pi_{n,\,m}}{\Pi_{n+1,\,m-1}} = \sqrt{\frac{2\,(2n+1)}{(n-m+2)\,(n-m+1)\,(2-\delta_{0,m-1})\,(2n+3)}} \tag{3.59}$$

$$\mathrm{X}^{(1,\,0)}_{n,\,m} \overset{m\geq 0}{=} \frac{\Pi_{n,\,m}}{\Pi_{n+1,\,m}} = \sqrt{\frac{(2n+1)\,(n+m+1)}{(n-m+1)\,(2n+3)}}\,. \tag{3.60}$$

The partial accelerations calculated with normalized coefficients are then given by

$$\begin{aligned}\ddot{x}_{n,\,0} &= -\frac{GM}{\overline{\mathrm{R}}^2}\,\overline{\mathrm{C}}_{n,\,0}\,\mathrm{X}^{(1,\,1)}_{n,\,0}\,\overline{\mathrm{V}}_{n+1,\,1} \\ &= -\frac{GM}{\overline{\mathrm{R}}^2}\,\sqrt{\frac{(2n+1)\,(n+1)\,(n+2)}{2\,(2n+3)}}\,\big(\overline{\mathrm{C}}_{n,\,0}\overline{\mathrm{V}}_{n+1,\,1}\big) \end{aligned} \tag{3.61a}$$

$$
\begin{aligned}
\ddot{x}_{n,\,m} \overset{m\geq 0}{=} & -\frac{1}{2}\frac{GM}{\overline{\mathrm{R}}^2}\Big(\overline{\mathrm{C}}_{n,\,m}\,\mathrm{X}^{(1,\,1)}_{n,\,m}\,\overline{\mathrm{V}}_{n+1,\,m+1}+\overline{\mathrm{S}}_{n,\,m}\,\mathrm{X}^{(1,\,1)}_{n,\,m}\,\overline{\mathrm{W}}_{n+1,\,m+1} \\
& -\,(n-m+2)\,(n-m+1)\,\Big(\overline{\mathrm{C}}_{n,\,m}\,\mathrm{X}^{(1,\,-1)}_{n,\,m}\,\overline{\mathrm{V}}_{n+1,\,m-1} \\
& +\overline{\mathrm{S}}_{n,\,m}\,\mathrm{X}^{(1,\,-1)}_{n,\,m}\,\overline{\mathrm{W}}_{n+1,\,m-1}\Big)\Big) \\
= & -\frac{1}{2}\frac{GM}{\overline{\mathrm{R}}^2}\,\sqrt{\frac{2n+1}{2n+3}}\,\Big(\sqrt{(n+m+2)\,(n+m+1)}\,\Big(\overline{\mathrm{C}}_{n,\,m}\,\overline{\mathrm{V}}_{n+1,\,m+1} \\
& +\overline{\mathrm{S}}_{n,\,m}\,\overline{\mathrm{W}}_{n+1,\,m+1}\Big)-\sqrt{\frac{2\,(n-m+2)\,(n-m+1)}{2-\delta_{0,m-1}}} \\
& \Big(\overline{\mathrm{C}}_{n,\,m}\,\overline{\mathrm{V}}_{n+1,\,m-1}+\overline{\mathrm{S}}_{n,\,m}\,\overline{\mathrm{W}}_{n+1,\,m-1}\Big)\Big)
\end{aligned}
\tag{3.61b}
$$

$$
\begin{aligned}
\ddot{y}_{n,\,0} = & -\frac{GM}{\overline{\mathrm{R}}^2}\,\overline{\mathrm{C}}_{n,\,0}\,\mathrm{X}^{(1,\,1)}_{n,\,0}\,\overline{\mathrm{W}}_{n+1,\,1} = \\
= & -\frac{GM}{\overline{\mathrm{R}}^2}\,\sqrt{\frac{(2n+1)\,(n+1)\;\,(n+2)}{2\,(2n+3)}}\,\Big(\overline{\mathrm{C}}_{n,\,0}\,\overline{\mathrm{W}}_{n+1,\,1}\Big)
\end{aligned}
\tag{3.62a}
$$

$$
\begin{aligned}
\ddot{y}_{n,\,m} \overset{m\geq 0}{=} & -\frac{1}{2}\frac{GM}{\overline{\mathrm{R}}^2}\Big(\overline{\mathrm{C}}_{n,\,m}\,\mathrm{X}^{(1,\,1)}_{n,\,m}\,\overline{\mathrm{W}}_{n+1,\,m+1}-\overline{\mathrm{S}}_{n,\,m}\,\mathrm{X}^{(1,\,1)}_{n,\,m}\,\overline{\mathrm{V}}_{n+1,\,m+1} \\
& +\,(n-m+2)\,(n-m+1)\,\Big(\overline{\mathrm{C}}_{n,\,m}\,\mathrm{X}^{(1,\,-1)}_{n,\,m}\,\overline{\mathrm{W}}_{n+1,\,m-1} \\
& -\overline{\mathrm{S}}_{n,\,m}\,\mathrm{X}^{(1,\,-1)}_{n,\,m}\,\overline{\mathrm{V}}_{n+1,\,m-1}\Big)\Big) \\
= & -\frac{1}{2}\frac{GM}{\overline{\mathrm{R}}^2}\,\sqrt{\frac{2n+1}{2n+3}}\,\Big(\sqrt{(n+m+2)\,(n+m+1)}\,\Big(\overline{\mathrm{C}}_{n,\,m}\,\overline{\mathrm{W}}_{n+1,\,m+1} \\
& -\overline{\mathrm{S}}_{n,\,m}\,\overline{\mathrm{V}}_{n+1,\,m+1}\Big)+\sqrt{\frac{2\,(n-m+2)\,(n-m+1)}{2-\delta_{0,m-1}}} \\
& \Big(\overline{\mathrm{C}}_{n,\,m}\,\overline{\mathrm{W}}_{n+1,\,m-1}-\overline{\mathrm{S}}_{n,\,m}\,\overline{\mathrm{V}}_{n+1,\,m-1}\Big)\Big)
\end{aligned}
\tag{3.62b}
$$

$$
\begin{aligned}
\ddot{z}_{n,\,0} = & -\frac{GM}{\overline{\mathrm{R}}^2}\;(n+1)\;\overline{\mathrm{C}}_{n,\,0}\,\mathrm{X}^{(1,\,0)}_{n,\,0}\,\overline{\mathrm{V}}_{n+1,\,0} = \\
= & -\frac{GM}{\overline{\mathrm{R}}^2}\;(n+1)\;\sqrt{\frac{(2n+1)}{(2n+3)}}\,\overline{\mathrm{C}}_{n,\,0}\,\overline{\mathrm{V}}_{n+1,\,0}
\end{aligned}
\tag{3.63a}
$$

$$
\begin{aligned}
\ddot{z}_{n,\,m} \overset{m\geq 0}{=} & -\frac{GM}{\overline{\mathrm{R}}^2}\;(n-m+1)\;\mathrm{X}^{(1,\,0)}_{n,\,m}\,\Big(\overline{\mathrm{C}}_{n,\,m}\,\overline{\mathrm{V}}_{n+1,\,m}+\overline{\mathrm{S}}_{n,\,m}\,\overline{\mathrm{W}}_{n+1,\,m}\Big) \\
= & -\frac{GM}{\overline{\mathrm{R}}^2}\,\sqrt{\frac{(2n+1)\,(n+m+1)\,(n-m+1)}{(2n+3)}}\,\Big(\overline{\mathrm{C}}_{n,\,m}\,\overline{\mathrm{V}}_{n+1,\,m} \\
& +\overline{\mathrm{S}}_{n,\,m}\,\overline{\mathrm{W}}_{n+1,\,m}\Big)
\end{aligned}
\tag{3.63b}
$$

The acceleration $\ddot{\boldsymbol{r}}$ can be computed in Cartesian coordinates by adding the partial accelerations.

$$
\ddot{x}=\sum_{n=0}^{\infty}\sum_{m=0}^{n}\ddot{x}_{n,m}\;,\qquad \ddot{y}=\sum_{n=0}^{\infty}\sum_{m=0}^{n}\ddot{y}_{n,m}\;,\qquad \ddot{z}=\sum_{n=0}^{\infty}\sum_{m=0}^{n}\ddot{z}_{n,m}\;. \tag{3.64}
$$

CHAPTER 4

Non-gravitational forces acting on a spacecraft

The orbit of a spacecraft is not only driven by gravitational forces but modified also by solar radiation pressure, atmospheric drag and other effects acting on a spacecraft. These forces will be described in detail in the following without claiming to be complete.

4.1 Solar radiation pressure

The Sun emits light energy (photons) depending on solar activity. During periods of intense solar storms the radiation is very strong and the force caused by the radiation at times of low activity very small. The body of a spacecraft absorbs and reflects photons which causes small forces changing the orbit of the spacecraft. The magnitude of the acceleration is inversely proportional to the squared distance of the spacecraft from the Sun.

The solar radiation pressure depends on the number of incoming photons and on their energy. The energy of a photon is given by $h \cdot f$, where h is Plank's constant and f the frequency of the photon. The solar flux q_s is defined as solar energy ΔE_f per time unit Δt which passes through the area A. Hence, the force acting on the spacecraft can be written:

$$\boldsymbol{F}_R = \frac{\Delta p}{\Delta t} = \frac{q_s}{c} A \,, \tag{4.1}$$

where c is the speed of light and Δp the impulse of the photon. The resulting radiation

pressure is

$$\boldsymbol{P}_R = \frac{q_s}{c}. \tag{4.2}$$

The solar flux at a distance of $r_0 = 1$ Astronomical Unit (AU) is approximately 1367 W/m^2 (*Montenbruck and Gill* [2000]). The solar radiation pressure is $\boldsymbol{P}_R = 4.56{\times}10^{-6}\frac{\mathrm{N}}{\mathrm{m}^2}$. However, this is only the case if the surface absorbs all incoming photons and the incident radiation is perpendicular to the surface.

In Figure 4.1 a more general case is shown. Here A_{exp} is the exposed surface which is inclined to the incoming radiation by the incident angle ϕ_{inc}. Fractions of the incoming radiation are absorbed and reflected. Reflection can take place specular, i.e. the incident angle ϕ_{inc} equals the reflection angle ϕ_{ref}, or diffuse, if this is not the case (see Figure 4.1). The fraction of specular or diffuse reflected radiation depends on the roughness of the surface, i.e. the optical properties of the spacecraft.The resulting accelerations caused by absorption, specular and diffuse reflection are according to *Milani et al.* [1987]:

$$\ddot{\boldsymbol{r}}_{abs} = -\frac{q_s}{c}\cos\left(\phi_{inc}\right)\frac{A_{exp}}{m_{\mathrm{SC}}}\,\boldsymbol{e}_{\odot} \tag{4.3a}$$

$$\ddot{\boldsymbol{r}}_{spec} = -2\frac{q_s}{c}\cos^2\left(\phi_{inc}\right)\frac{A_{exp}}{m_{\mathrm{SC}}}\,\boldsymbol{e}_N \tag{4.3b}$$

$$\ddot{\boldsymbol{r}}_{dif} = -\frac{q_s}{c}\cos\left(\phi_{inc}\right)\frac{A_{exp}}{m_{\mathrm{SC}}}\left(\boldsymbol{e}_{\odot} + \frac{2}{3}\,\boldsymbol{e}_N\right). \tag{4.3c}$$

Here, vector $\boldsymbol{e}_{\odot}$ is the unit vector in the direction of the sun and $\boldsymbol{e}_N$ the vector normal to the surface. Introducing coefficients α, δ and ε describing the fraction of absorbed, diffuse and specular reflected radiation ($\alpha + \delta + \varepsilon = 1$) and combining equation (4.3a), (4.3b) and (4.3c), the acceleration due to the solar radiation pressure felt by a satellite with mass m_{SC} at a distance $r_{\odot}$ from the Sun can be written as

$$\ddot{\boldsymbol{r}} = -k\frac{q_s}{c}\frac{r_0^2}{r_{\odot}^2}\cos\left(\phi_{inc}\right)\frac{A_{exp}}{m_{\mathrm{SC}}}\left(\left(\alpha+\delta\right)\,\boldsymbol{e}_{\odot} + 2\left(\varepsilon\cos\left(\phi_{inc}\right) + \delta\frac{1}{3}\right)\,\boldsymbol{e}_N\right). \tag{4.4}$$

Here r_0 is 1 AU. The activity of the Sun, i.e. the solar flux is not constant over time, which is accounted for by introducing a scaling factor k. This scaling factor is usually treated as a free parameter in the orbit determination process.

Equation (4.4) can be simplified if it is assumed that the surface normal $\boldsymbol{e}_N$ always points in the direction of the Sun and if no detailed information about the optical properties of the spacecraft is available:

$$\ddot{\boldsymbol{r}} = -k\frac{q_s}{c}\frac{r_0^2}{r_{\odot}^2}\frac{A_{exp}}{m_{\mathrm{SC}}}\,\boldsymbol{e}_{\odot} \tag{4.5}$$

This expression can also be used if no high precision is acquired.

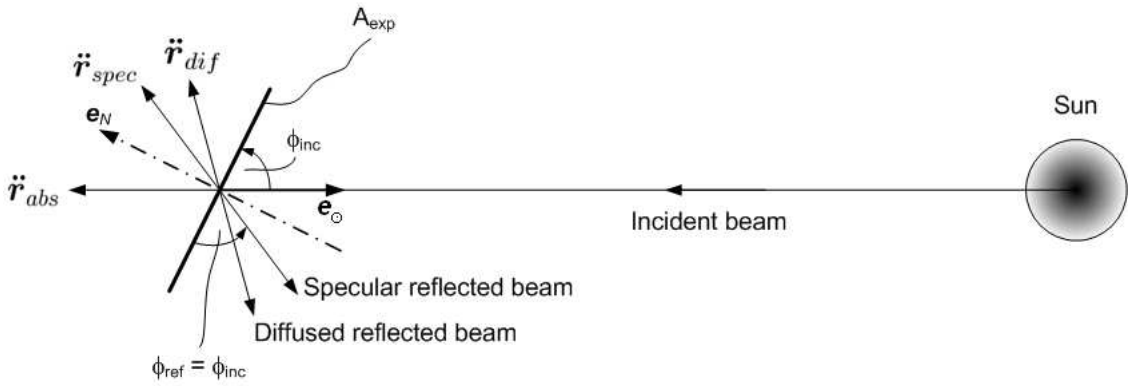

Figure 4.1: *The incident radiation results in accelerations $\ddot{\boldsymbol{r}}_{abs}$, $\ddot{\boldsymbol{r}}_{spec}$ and $\ddot{\boldsymbol{r}}_{dif}$ caused by absorption, specular and diffuse reflection*

4.2 Shadow function

The acceleration given by equation (4.4) assumes full illumination of the satellite by the Sun. In a realistic scenario it is possible that the satellite disappears behind the planet as seen from the Sun and therefore is not or only partially exposed to the solar radiation pressure. This problem can be solved by introducing a shadow function ν, which is defined as follows

$$\begin{aligned} \nu &= 0 \text{ , if the satellite is behind the planet and entirely in the shadow,} \\ \nu &= 1 \text{ , if the satellite is fully illuminated by the Sun, and} \\ 0 &< \nu < 1 \text{ partially illuminated by the Sun.} \end{aligned}$$

Montenbruck and Gill [2000] developed analytical expressions for illumination conditions from a conical shadow model. The apparent radius of the occulted body (the Sun) a, the apparent radius of the occulting body (the planet) b and the apparent separation of the centers of both bodies c can be obtained via the following equations.

$$a = \arcsin \frac{R_\odot}{|\boldsymbol{r}_\odot - \boldsymbol{r}|} \tag{4.6}$$

$$b = \arcsin \frac{R_B}{s} \tag{4.7}$$

$$c = \arccos \frac{-\boldsymbol{s}^T (\boldsymbol{r}_\odot - \boldsymbol{r})}{s\,|\boldsymbol{r}_\odot - \boldsymbol{r}|} \tag{4.8}$$

Here, $R_\odot$ is the Radius of the Sun (696000 km), $\boldsymbol{r}_\odot$ the coordinates of the Sun, $\boldsymbol{r}$ the coordinates of the spacecraft, R_B the radius of the occulted body, and $\boldsymbol{s}$ the vector from spacecraft to occulted body. The occulted array is then

$$A = a^2 \cdot \arccos\left(\frac{x}{a}\right) + b^2 \cdot \arccos\left(\frac{c-x}{b}\right) - c \cdot y, \tag{4.9}$$

with

$$x = \frac{a^2 + c^2 - b^2}{2c} \tag{4.10}$$

$$y = \sqrt{a^2 - x^2}. \tag{4.11}$$

Hence, the remaining fraction of the radiation on the spacecraft is

$$\nu = 1 - \frac{A}{\pi a^2}\,. \tag{4.12}$$

Accordingly, the resulting acceleration from the solar radiation pressure (see equation (4.4)) felt by the spacecraft is

$$\ddot{\boldsymbol{r}} = -\nu k \frac{q_s}{c} \frac{r_0^2}{r_\odot^2} \cos(\phi) \frac{A_{exp}}{m_{\mathrm{SC}}} \left((\alpha + \delta)\ \boldsymbol{e}_\odot + 2 \left(\varepsilon \cos(\phi) + \delta \frac{1}{3} \right) \boldsymbol{e}_N \right). \tag{4.13}$$

4.3 Atmospheric drag

A spacecraft orbiting a planet encounters air molecules from the planet's atmosphere. The change in the molecules' momentum due to collision with the spacecraft leads to a force acting on the spacecraft, called atmospheric drag. This force depends on the local density of the atmosphere and the surface area of the spacecraft exposed in the direction of motion (*Montenbruck and Gill* [2000])

$$\ddot{\boldsymbol{r}}_D = -\frac{1}{2} C_D \frac{A_{exp}}{m_{\mathrm{SC}}} \rho v_r^2 \boldsymbol{e}_v\,, \tag{4.14}$$

where ρ is the atmospheric density, v is the velocity of the spacecraft relative to the atmosphere and C_D is the drag coefficient, a dimensionless quantity, which describes the interaction between the surface material of the spacecraft and the atmosphere. Usually C_D or the ballistic coefficient $C_D \frac{A_{exp}}{m_{\mathrm{SC}}}$ is estimated in the orbit determination process as a free parameter. The unit vector $\boldsymbol{e}_v = \frac{\boldsymbol{v}_r}{v_r}$ allows for the fact that the direction of the drag acceleration is always anti-parallel to the relative velocity vector $\boldsymbol{v}_r$. The relative velocity of the spacecraft can be computed under the assumption that the atmosphere co-rotates with the planet

$$\boldsymbol{v}_r = \boldsymbol{v} - \boldsymbol{\omega} \times \boldsymbol{r}\,, \tag{4.15}$$

with the inertial velocity vector of the spacecraft $\boldsymbol{v}$, the position vector $\boldsymbol{r}$ and the angular velocity of the planet $\boldsymbol{\omega}$. The atmospheric density can be computed either from standard atmospheric models or from dynamic models. It is also necessary to use a precise model for the spacecraft as it is used for the solar radiation pressure modeling.

4.4 Albedo and infrared radiation

The incoming solar radiation reflected and scattered from a body is called albedo radiation. The optical albedo indicates the ability of reflection and scattering of the incident solar radiation, i.e. the ratio of reflected and incoming radiation, and is usually given in percent of the reflected radiation from the body. In addition, planetary surfaces and atmospheres emit infrared radiation, which also contributes to the radiation pressure felt by an orbiting spacecraft.

Montenbruck and Gill [2000] gives a formulation which accounts for the acceleration acting on a spacecraft due to optical and infrared radiation summing up individual terms, corresponding to different area elements dA_j of the planet

$$\ddot{\boldsymbol{r}}_{rad} = \sum_{j=1}^{N} C_R \left(\nu_j a_j \cos\theta_j^E + \frac{1}{4}\epsilon_j \right) \frac{q_s}{c} \frac{A_{exp}}{m_{\mathrm{SC}}} \cos\theta_j^S \frac{dA_j}{\pi r_j^2} \boldsymbol{e}_j \,. \tag{4.16}$$

Here, C_R is the radiation pressure coefficient of the spacecraft, ν_j the shadow function for the planets area element dA_j, a_j the albedo, ϵ_j the emissivity, θ_j^E and θ_j^S the angles of the planet surface or spacecraft surface normals to the incident radiation, $\frac{q_s}{c}$ the radiation pressure, r_j the distance between planet and spacecraft, and $\boldsymbol{e}_j$ the unit vector from the surface to the spacecraft.

4.5 Thrust forces

In order to control the orbit and the attitude of spacecraft the thruster-system on board a spacecraft has to applied. For a detailed orbit determination this effect has to be accounted for. Thrusters are burned best in pairs to produce a pure momentum-free torque. Thrusters are acting primarily in the along-track and cross-track direction. Maneuvers can be treated as instantaneous velocity increments taking place at time t_m

$$\boldsymbol{v}\left(t_m^+\right) = \boldsymbol{v}\left(t_m^-\right) + \Delta\boldsymbol{v}\left(t_m\right) \,. \tag{4.17}$$

Dealing with extend maneuvers needs a complex thrust model but in the following only a simple model based on constant thrust is shown (*Montenbruck and Gill* [2000]). A spacecraft of mass m experiencing a thrust acceleration assuming a one dimensional motion

$$a = \frac{F}{m} = \frac{|\dot{m}|\, c_e}{m}, \tag{4.18}$$

with propellant mass $|dm| = |\dot{m}|\, dt$ ejected from the propulsion system per time dt at velocity c_e.

The entire velocity increment can be computed by integration over the burn time Δt

$$\begin{aligned} \Delta v &= \int_{t_0}^{t_0+\Delta t} a(t)dt = -c_e \int_{m(t_0)}^{m(t_0+\Delta t)} \frac{1}{m} dm \\ &= -c_e \, ln \frac{m\,(t_0+\Delta t)}{m\,(t_0)}\,, \end{aligned} \tag{4.19}$$

which is the Ziolkowski equation. Assuming a constant mass-flow rate $|\dot{m}|$, the entire velocity increment is

$$\Delta v = -\frac{F}{[\dot{m}]}\, ln\left(1 - \frac{|\dot{m}|\,\Delta t}{m\,(t_0)}\right)\,. \tag{4.20}$$

Using equation (4.18) and (4.20) the resulting acceleration is then

$$a(t) = \frac{|\dot{m}|}{m\,(t)} \frac{1}{-ln\left(1 - \frac{|\dot{m}|\Delta t}{m(t_0)}\right)} \Delta v. \tag{4.21}$$

Introducing a time-dependent set of orthogonal unit vectors $\boldsymbol{e}_1$, $\boldsymbol{e}_2$, $\boldsymbol{e}_3$ with constant projected thrust vector components F_1, F_2 and F_3 the resulting acceleration in the inertial reference frame is given by

$$\boldsymbol{a}(t) = \frac{|\dot{m}|}{m\,(t)} \frac{1}{-ln\left(1 - \frac{|\dot{m}|\Delta t}{m(t_0)}\right)} \boldsymbol{E}\Delta\boldsymbol{v}\,(t)\,, \tag{4.22}$$

where $\Delta\boldsymbol{v}\,(t)$ are the velocity increments in the thrust reference frame and the rotation matrix $\boldsymbol{E}\,(t) = (\boldsymbol{e}_1, \boldsymbol{e}_2, \boldsymbol{e}_3)$ transforms the acceleration from the thrust reference frame into the inertial frame.

In the case of a negligible mass flow $|\dot{m}|\,\Delta t \ll m\,(t_0)$ the resulting acceleration can be simplified to

$$\boldsymbol{a}(t) = \frac{1}{m}\boldsymbol{E}\,(t) \begin{pmatrix} F_1 \\ F_2 \\ F_3 \end{pmatrix}. \tag{4.23}$$

CHAPTER 5

The relativistic Doppler effect

If a spacecraft is transmitting an electromagnetic wave with frequency f_T and on Earth the signal is received via a ground station with frequency f_R, the relativistic Doppler effect taking into account effects if special relativity of order $\left(\frac{v}{c}\right)^2$ and effects of the general relativity can be computed from the following equation (see Figure 5.1) according to *Häusler* [2002]

$$\frac{\Delta f}{f_T} = 1 - \frac{1 - \boldsymbol{n}\boldsymbol{\beta}_R + \frac{1}{2}\left|\boldsymbol{\beta}_R\right|^2 - \frac{\Phi_R}{c^2}}{1 - \boldsymbol{n}\boldsymbol{\beta}_T + \frac{1}{2}\left|\boldsymbol{\beta}_T\right|^2 - \frac{\Phi_T}{c^2}}. \tag{5.1}$$

Here,

- Δf is the Doppler frequency shift with $\Delta f = f_T - f_R$ where f_T is the transmitted frequency and f_R is the received frequency,
- $\boldsymbol{n}$ is the normalized vector from transmitter at transmission time t_T to receiver at receiving time t_R,
- $\boldsymbol{\beta}_T$ is the normalized velocity of transmitter with $\boldsymbol{\beta}_T = \frac{\boldsymbol{v}_T}{c}$, where $\boldsymbol{v}_T$ is the velocity of the transmitter at the time of transmission t_T,
- $\boldsymbol{\beta}_R$ is the normalized velocity of receiver with $\boldsymbol{\beta}_R = \frac{\boldsymbol{v}_R}{c}$, where $\boldsymbol{v}_R$ is the velocity of the receiver at the time of reception t_R,
- c is the speed of light,
- Φ_T is the gravity potential of the Sun and the planet in which sphere of influence the transmitter is located, with $\Phi_T = -\frac{\mu_\odot}{r_\odot} - \frac{\mu_p}{r_p}$ and $r_\odot$ the distance from the

transmitter to the Sun and r_p the distance from the transmitter to the planet, and

- Φ_R the gravity potential of the Sun and the planet in which sphere of influence the receiver is located, with $\Phi_R = -\frac{\mu_\odot}{r_\odot} - \frac{\mu_p}{r_p}$ and $r_\odot$ the distance from the receiver to the Sun and r_p the distance from the receiver to the planet.

If the receiver or transmitter is located on Earth the centrifugal acceleration from Earth rotation should also to be taken into account using the following equation

$$\Phi_c = -\frac{1}{2} \cdot \left(\omega_\otimes \sin\left(\frac{\Pi}{2} - \phi \right) r \right)^2, \tag{5.2}$$

whereas

- $\omega_\otimes$is the angular velocity of the Earth in radian per second,
- ϕ the geographical latitude of the ground station, and
- r distance from the center of the earth to the ground station.

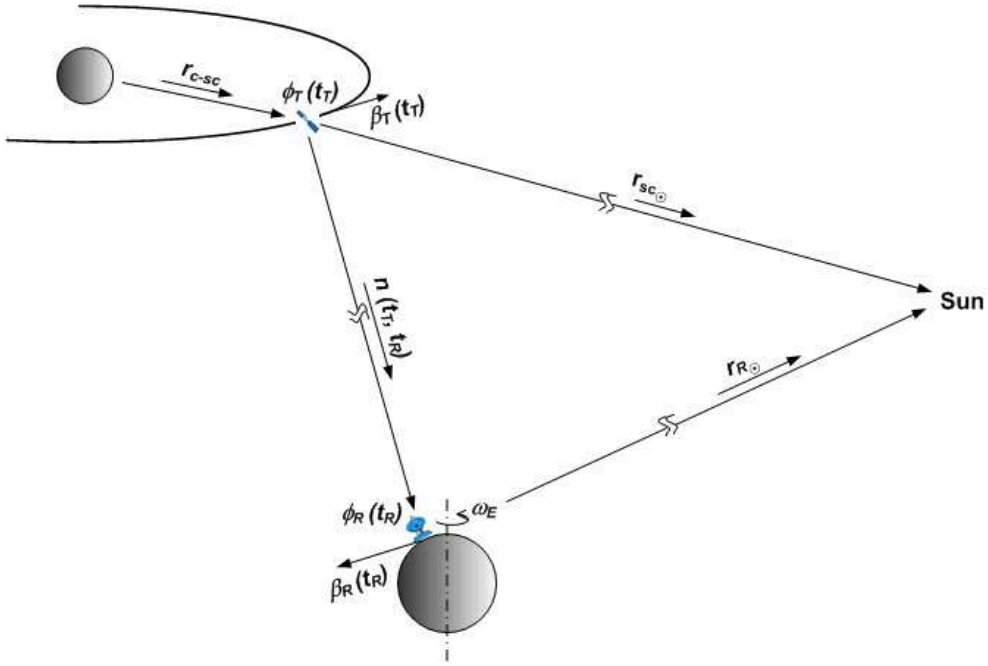

Figure 5.1: *Parameter fro the computation of the relativistic Doppler effect in the downlink case i.e. the spacecraft is transmitting a radio signal to the ground station located on Earth.*

Equation (5.1) requires the knowledge of the travel time of the radio signal from the instant of transmission to the instant of reception. These light time corrections are calculated iteratively starting from an initial value (assuming infinite speed of light) using a Newtonian formulation (*Häusler* [2002], *NAIF* [2009]).

In the literature other approximations can be found for the relativistic Doppler effect (*Morabito and Asmar* [1995], *Schneider* [1988], *Ashby* [2003] or *Soffel* [1989]). However the differences between the different expressions for the relativistic Doppler effect is in the range of a few mHz (*Selle* [2005]). The precision of the used formulation (5.1) is tested in section **??**.

5.1 Relativistic summation

If the normalized velocity in equation 5.1 is computed barycentric and planetocentric velocities have to be added but it has to be taken care that nothing moves faster than light. Therefore the velocities have to be summed up in a relativistic way.

Assuming a system S' moving relative to system S with the velocity $\boldsymbol{u}$ and an observer is situated in the system S. A body is assumed to have the velocity $\boldsymbol{v'}$ in system S'. Calculating the velocity $\boldsymbol{v}$ of the body in system S in a non-relativistic way can be done via

$$\boldsymbol{v} = \boldsymbol{v'} + \boldsymbol{u}. \tag{5.3}$$

However, if $|\boldsymbol{u}|$ and $|\boldsymbol{v'}| > \frac{c}{2}$ this would lead to $|\boldsymbol{v}| > c$. This can't be true, because the effects of time dilatation and contraction of the length requires the existence of a limited velocity not depending on the reference frame.

The time dilatation, i.e. the time interval between two events in the moving system S', seems to be extended for the observer in the resting frame S by the Lorenz term

$$\gamma = \frac{1}{\sqrt{1 - \left(\frac{u}{c}\right)^2}} \tag{5.4}$$

and the contraction of the length, i.e. the length of a distance in the moving system S', seems to be for the observer in the resting system S shortened by the factor $\frac{1}{\gamma}$.

The velocity in the system S is via relativistic summation (see *Dorfmüller et al.* [1998])

$$\boldsymbol{v} = \frac{1}{\gamma\left(1 + \boldsymbol{\beta_u} \cdot \boldsymbol{\beta_{v'}}\right)}\left(\boldsymbol{v'} + (\gamma - 1)\left(\boldsymbol{v'} \cdot \check{\boldsymbol{u}}\right)\check{\boldsymbol{u}} + \gamma \boldsymbol{u}\right), \tag{5.5}$$

whereas

- $\check{\boldsymbol{u}}$ is the unit vector of the velocity $\boldsymbol{u}$ of the system S' relative to system S,
- $\boldsymbol{\beta_u}$ the normalized velocity of the system S' relative to system S, i.e. $\frac{\boldsymbol{u}}{c}$, and
- $\boldsymbol{\beta_{v'}}$ the normalized velocity of the body in system S', i.e. $\frac{\boldsymbol{v'}}{c}$.

5.1.1 Precise ground station position

The precise modeling of the Doppler effect requires an accurate knowledge at centimeter level of the position of the ground station on the surface of the Earth. The crust of the Earth is variable and reference points are displaced by linear effects like the tectonic plate motion and non-linear effects like the solid Earth tides. Methods to model this effects are described in the following.

In the celestial reference frame for a precise ground station position effects due to precession, nutation, Earth rotation, and polar motion have to be taken into account. In section 2.3 the transformation from the celestial to the terrestrial coordinate system is described in which the effects are considered.

5.1.2 Tectonic plate motion

The lithosphere of the Earth is divided laterally into a number of tectonic plates. Twelve major plates and several minor plates exist. The tectonic plates are moving relative to each other and a comprehensive model of current plate motions shows rates of separation at plate boundaries that range from 20 mm/year in the North Atlantic to about 160 mm/year on the East Pacific Rise. The model also gives rates of closure ranging from about 10 mm/year between Africa and Eurasia to about 80 mm/year between the Naza plate and South America.

Depending on the location of the ground station the site displacement from tectonic plate motion has to be considered for a precise ground station position. The NNR-NUVEL1A model for plate motions (see *McCarthy and Petit* [2003]) can be used for

modeling. From the original coordinates $\boldsymbol{r_0} = (x_0, y_0, z_0)$ in the International Terrestrial Reference Frame (ITRF) (see section 2) at time t_0 new coordinates $\boldsymbol{r} = (x, y, z)$ at time t can be computed from the Cartesian rotation vector $\boldsymbol{\Omega}$ via

$$x = x_0 + (\Omega_y z_0 - \Omega_z y_0)(t - t_0) \tag{5.6}$$
$$y = y_0 + (\Omega_z x_0 - \Omega_x z_0)(t - t_0) \tag{5.7}$$
$$z = z_0 + (\Omega_x y_0 - \Omega_y x_0)(t - t_0)\,. \tag{5.8}$$

The values of the rotation vector $\boldsymbol{\Omega}$ for each of the major plates can be found in Table A.2 in the appendix.

5.1.3 Site displacement due to solid Earth tides

Tidal forces arise from gravitational attraction of bodies external to the Earth. The resulting deformation of the shape of the non perfectly rigid Earth causes site displacements. The tidal acceleration at a point on or in the Earth is the difference between the acceleration caused by the attraction of the external body and the orbital acceleration. Assuming the Earth being spherical symmetric, the orbital acceleration is the acceleration caused by the attraction of the external body at the Earth's center of mass, making the tidal force the difference between the attraction at the center of mass, and that at the point of observation. The tidal potential can be expressed as (*Agnew* [2007])

$$V_{tid} = \frac{GM_{ex}}{R(t)} \sum_{n=2}^{\infty} \left(\frac{a}{R(t)} \right)^n \frac{4\pi}{2n+1} \sum_{m=-n}^{n} Y^*_{nm}(\theta'(t), \phi'(t))\, Y_{nm}(\theta, \phi)\,. \tag{5.9}$$

Here, M_{ex} is the mass of the external body, $R(t)$ the distance between the center of mass of the Earth and the center of mass of the external body, a the distance of the observation point on Earth from the center of mass of the Earth, θ, ϕ the colatitude and east longitude of the observation point, and $\theta'(t)$, $\phi'(t)$ the colatitude and east longitude of the sub-body point of the center of mass of the external body and $Y_{nm}(\theta, \phi)$ the fully normalized complex spherical harmonics defined by

$$Y_{nm}(\theta, \phi) = N_n^m P_n^m(\cos\theta)\, e^{im\phi}\,. \tag{5.10}$$

Here,

$$N_n^m = (-1)^m \left[\frac{2n+1}{4\pi} \frac{(n-m)!}{(n+m)!} \right]^{\frac{1}{2}} \tag{5.11}$$

is the normalizing factor and P_n^m is the associated Legendre polynomial of degree n and order m. The solid tides can be expressed as a sum of sinusoids as

$$T_{nm} = \sum_{k=1}^{k_{nm}} A_{knm} e^{i(2\pi f_{knm} t + \varphi_{knm})}\,, \tag{5.12}$$

where, for each degree n and order m k_{nm} sinusoids with specified real amplitudes A, frequencies f, and phases φ are summed. A table of harmonic amplitudes and frequencies can be used to model the tidal potential. This method can be used for Earth tides of any type (*Agnew* [2007]).

McCarthy and Petit [2003] developed a numerical two-step procedure using the sum of sinusoids in order to model site displacements caused by solid tides which will be described only briefly here because of its complexity.

In the first step corrections in the time domain are computed, i.e. the in-phase correction for degree 2 and 3, the out-of-phase correction for degree 2 only of the diurnal and semidiurnal tides and the contribution from the latitude dependence of the diurnal and semidiurnal tides. The second step comprises estimating corrections in the frequency domain, i.e. the in-phase correction for degree 2 of the diurnal and semidiurnal tides and the in-phase and out-of-phase correction of degree 2 of the long-period tides. This model is used in this thesis for computing the site displacement effects due to solid Earth tides.

5.1.4 Other effects

There are additional effects which are changing the position of a ground station. Here, some of them are briefly described and summarized in Table 5.1 without claiming completeness.

- **Ocean loading**

  The site displacement due to ocean loading is mainly in the horizontal direction. It is due to temporal variations of the ocean mass distribution and the associated load on the crust, which produces time-varying deformations of the Earth. Ground stations close to the coast or on islands are affected strongest. The effect has periods about 12 hours, 24 hours, 14 days, but also monthly and half year periods due to Sun and moon. The amplitude is smaller than that of the solid tides and in the range of a few centimeter.

- **Atmospheric loading**

  The surface of the Earth is deformed by temporal variations in the geographic distribution of atmospheric mass load. The mass load variations can originate from pressure variations, for example seasonal pressure changes due to air mass movements between the continents and oceans. Other surface loads caused by changes in snow and ice cover, soil moisture and groundwater, as well as ocean bottom pressure also contribute to surface displacements, but for the latter ones no sufficient models are available. The atmospheric load from pressure variations can be modeled via two basic methods. Firstly, computing the corrections based on geophysical models or simple approximations or, secondly, using empirical

models based on site dependent data like meteorological data measured at the ground station. The order of magnitude of the effect due to atmospheric loading on the location of a ground station is approximately a few millimeter.

- **Thermal deformation of the antenna**

  The structure of an antenna can be deformed depending on the temperature and can therefore cause errors in the position of the antenna. These errors are in the range of a few millimeter.

- **Postglacial rebound**

  This is due to the slowly raising of the crust of the Earth since the polar caps are melt and the maximum is in the range of millimeter per year.

The order of magnitude of these effects are all in the range of centimeter or smaller (Table 5.1). With the complexity of the models, the effort of modeling this effects can not be justified with the higher accuracy and would go beyond the scope of this work. In the software plate tectonic and solid Earth tides effects are implemented in the computation of the ground station position which serves an accuracy at the centimeter level. A detailed description of the effects of site displacements and their accurate numeric modeling is given in *McCarthy and Petit* [2003].

Effect	**Order of magnitude**
Tectonic plate motion	cm/year
Solid Tides	dm
Ocean Tide Loading	cm
Pole Tides	mm - cm
Atmospheric Loading	mm
Thermal deformation of the antenna	mm
Postglacial rebound	mm/year

Table 5.1: *Summary of the order of magnitude for site displacement effects (Hennig [2008]).*

CHAPTER 6

Data calibration

6.1 Introduction

An electromagnetic wave emitted from the spacecraft in order to be received at ground station and vice versa passes the atmosphere of the Earth. Thereby the wave interacts with electrons, ions, atoms and molecules contained in the Earth atmosphere and plasma environment. Thus the direction and velocity of propagation and also the polarization and the field strength of the signal is changed.

The velocity and the wavelength of an electromagnetic wave depends on the refractive index n of the surrounding media and is related by the following equation

$$n = \frac{c}{c_n} = \frac{\lambda}{\lambda_n}, \tag{6.1}$$

where c is the speed of light, λ the vacuum wavelength, and c_n, λ_n are the corresponding values in media with refractive index n. The refractive index depends mainly on the dielectric constant, the permeability, and the conductivity of the medium.

Assuming a simplified model of a plane atmosphere with a constant refractivity the basic effect of the atmospheric refraction can be described by Snellius's law

$$n \sin(z) = \sin(z_0). \tag{6.2}$$

Here z_0 is the zenith angle, i.e. the angle of the incoming ray and z the angle in the medium with refractive index n. The signal traversing the atmosphere is bended and due to the reduced velocity inside the atmosphere, if $n > 1$, a signal is delayed in time. Neglecting the small bending angle at Earth the path delay $\Delta\tau$ caused in a layer with height h and refractive index n of the atmosphere is then

$$\Delta\tau = h\,(n-1)\,\frac{1}{\sin\epsilon}, \tag{6.3}$$

where $\epsilon = 90\,^\circ - z_0$ is the elevation angle (*Montenbruck and Gill* [2000]). The troposphere of the Earth is a non-dispersive media for radio waves, i.e. the refractive index is independent from frequency, but for the ionospheric correction it must be distinguished between the refractive index of a single electromagnetic wave (e.g. the carrier phase) and wave groups (e.g. ranging signals).

The changes in signal path, i.e. frequency changes of the radio signal by the contributions of the troposphere and ionosphere of the Earth have to be removed accurately from the data in order to obtain the frequency, i.e. the Doppler velocity, due to the motion of a spacecraft. Different models for these corrections are shown in the following.

6.2 Modeling tropospheric delays

The troposphere of the Earth ranging from the sea surface level to approximately 8 km at the pole and 16 at the equator consists almost completely of neutral gas. The propagation of electromagnetic waves is mainly affected by the temperature T, the atmospheric pressure P and the partial pressure of water vapour e. The tropospheric refractive index is always larger than one. The tropospheric refraction consists of the refraction caused by the nonwater-vapor components of the atmosphere (N_2, O_2, CO_2, and Ar), the dry component, and the contribution of the highly variable water vapour content of the atmosphere, the wet component. Both have to be modeled separately. The tropospheric delay can be computed in general from

$$\tau_{tropo} = \delta_d m_d(\epsilon) + \delta_w m_w(\epsilon) \ . \tag{6.4}$$

In the following models for the path delay δ_d and δ_w in the zenith direction and the mapping functions $m_d(\epsilon)$ and $m_w(\epsilon)$ projecting the delay into the direction of the signal path for both components are shown.

The tropospheric correction models using the temperature T in Kelvin, the pressure P in hPa, the partial water vapour pressure e at ground station in hPa, the latitude ϕ of the ground station and the height h of the ground station above the reference ellipsoid in km.

6.2.1 Zenith delay

Dry component:

- Model from *Janes et al.* [1991]

$$\delta_d = 1.552 \times 10^{-5} \left[\frac{\mathrm{m}}{\mathrm{hPa}}\right] \frac{P}{T} \left(40136\,[\mathrm{K}] + 148.72\,(T - 273.15\,[\mathrm{K}])\right) \tag{6.5}$$

- Model from *Saastamoinen* [1972]

$$\delta_d = \frac{2.2767 \times 10^{-3} \left[\frac{\mathrm{m}}{\mathrm{hPa}}\right] P}{1 - 2.66 \times 10^{-3} \left[\frac{1}{\mathrm{km}}\right] \cos(2\phi) - 2.8 \times 10^{-4} \cdot h} \tag{6.6}$$

Wet component

- Model from *Mendes and Langely* [1998]

$$\delta_w = 0.122\,[\mathrm{m}] + 9.45 \times 10^{-3} \left[\frac{\mathrm{m}}{\mathrm{hPa}}\right] e \tag{6.7}$$

- Model from *Ifadis* [1986]

$$\begin{aligned}\delta_w &= 5.54 \times 10^{-3}\,[\mathrm{m}] - 8.8 \times 10^{-5}\left[\frac{\mathrm{m}}{\mathrm{hPa}}\right](P - 1000\,[\mathrm{hPa}]) \\ &\quad +2.72 \times 10^{-5}\left[\frac{\mathrm{m}}{\mathrm{hPa}}\right] e + 2.771\left[\frac{\mathrm{m\,K}}{\mathrm{hPa}}\right]\frac{e}{T} \end{aligned} \tag{6.8}$$

6.2.2 Mapping functions

The mapping function projects the path delay in zenith direction into the direction of the signal path according to the elevation angle ϵ.

Dry component:

- Mapping function from *Chao* [1972]

$$m_d(\epsilon) = \frac{1}{\sin\epsilon + \frac{0.00143}{\tan\epsilon + 0.00035}} \tag{6.9}$$

Wet component:

- Mapping function from *Chao* [1972]

$$m_w(\epsilon) = \frac{1}{\sin\epsilon + \frac{0.00035}{\tan\epsilon + 0.0017}} \tag{6.10}$$

6.2.3 Comparison

Janes et al. [1991] compared the results from the ray-tracing method with different models for tropospheric delay prediction using a standard atmosphere. The ray-tracing technique divides the atmosphere into small layers with respective refraction index and computes the ray path of the signal separately for each layer using Snellius's law. Therefore results from this method can be used for testing the accuracy of tropospheric delay predictions from the different models. *Janes et al.* [1991] found that the zenith delay model for the dry component from *Saastamoinen* [1972] agrees well within a few millimeters, but models for the wet component show differences in the centimeter level with the ray-tracing results. A comparison of ray-tracing results with several mapping functions performed by *Mendes and Langely* [1994] show agreements for all tested mapping functions in the sub-centimeter level.

This agreement can also be confirmed comparing the above defined models as it can be seen in Figure 6.1(a) for the dry component and in Figure 6.1(b) for the wet component. The path delay of the models are projected into the direction of the signal using the mapping functions according to equations 6.9 and 6.10.

For data analysis the model from *Saastamoinen* [1972] for the dry component and from *Ifadis* [1986] for the wet component, and the straightforward mapping functions from *Chao* [1972] are used.

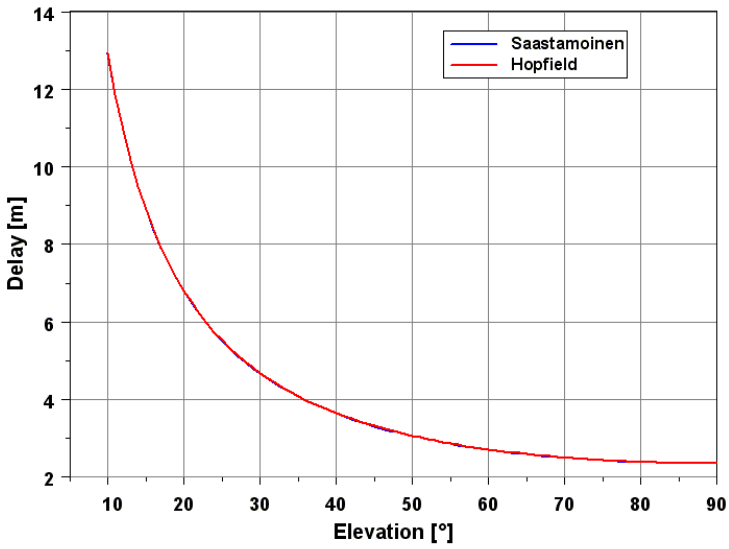

(a) Dry component

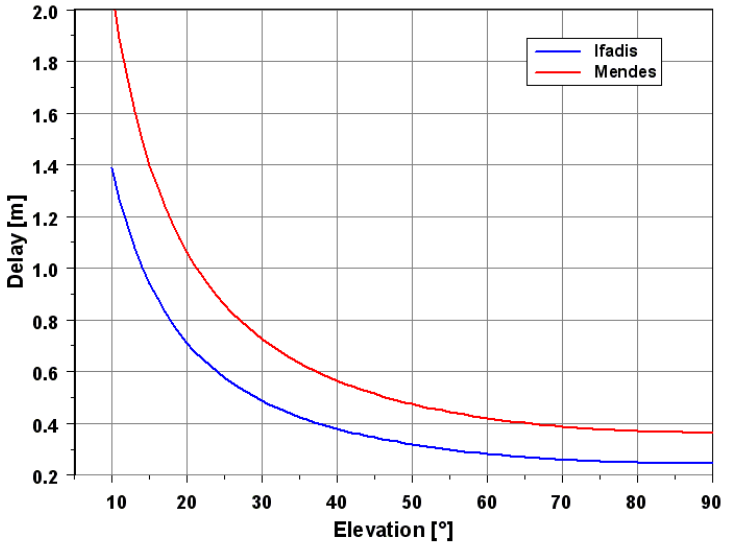

(b) Wet component

Figure 6.1: *Comparison of different models for the dry and wet component of the signal path delay caused by the troposphere of the Earth. Used for modeling are temperature $T = 295.5$ K, pressure $P = 978.0$ hPa and humidity $H = 66$ %. The mapping functions are according to equation* (6.9) *and* (6.10)

6.3 Ionospheric correction

The ionosphere of the Earth ranges from 50 km to 1000 km. The source of the ionospheric refraction, the ions and free electrons are mainly generated by the absorption of ultra violet radiation from the Sun. Different regions can be distinguished by the electron density: the D region (60 - 90 km), the E region (105 - 160 km) and the F region (160 - 500 km), which can be subdivided into the F_1 region (160 - 180 km) and the F_2 region (200 - 500 km). The D and F_1 region vanish at night, while the E region becomes considerably weaker and the F_2 region is also reduced. At an altitude of 300 km a maximum electron density of about 10^{12} electrons/m^3 can be found.

The ionosphere is a dispersive medium, i.e. the refractive index is a function of the frequency of the signal. Neglecting the perturbations due to ions, the contributions from the magnetic field of the Earth, and absorption effects, the ionospheric refractive index is (*Häusler* [2008*b*])

$$n = 1 - \frac{1}{2}\frac{f_p^2}{f^2}. \tag{6.11}$$

Here, f_p denotes the plasma frequency varying from 10 MHz at day to 3 MHz at night

$$f_p = \frac{1}{2\pi}\sqrt{\frac{d_e e_0^2}{m_e \epsilon_0}}, \tag{6.12}$$

with the electron number density d_e, the electron charge e_0, the vacuum dielectric constant ϵ_0, and the electron mass m_e. The ionospheric refraction leads to a reduction of the group velocity and an increase of the phase velocity. Both corrections for range and carrier phase measurements $\Delta\rho$ and $\Delta\phi$ are

$$\Delta\rho = \int_0^S (n-1)\,ds = \frac{40.31\left[\frac{m^3}{s^2}\right]}{f^2}\,TEC \tag{6.13}$$

$$\Delta\phi\lambda_0 = 2\pi\int_0^S (n-1)\,ds = -2\pi\frac{40.31\left[\frac{m^3}{s^2}\right]}{f^2}\,TEC. \tag{6.14}$$

Here is TEC the total electron content along the path length S. The electron density of the ionosphere varies with altitude, Sun activity and with local time. This makes it difficult to construct global ionospheric models that predict the electron density accurately. But the electron density can be measured and used for correction of the contributions of the ionosphere on an electromagnetic wave. For Deep Space Network (DSN) ground stations the ionospheric correction can be reconstructed from auxiliary files provided by the Tracking System Analytic Calibration (TSAC) group of Jet Propulsion Laboratory (JPL). For measurements recorded at European Space Agency (ESA) ground stations another method has to be used because no information is provided by ESA about ionospheric corrections. Both methods are explained and compared below.

6.3.1 Correction provided by TSAC

The TSAC group of JPL provides the path delay signature in form of a polynomial which can be computed from the polynomial coefficients a_i via (see *Morabito and Asmar* [1995])

$$\Delta\rho_{ion}\left(t_j\right) = \sum_{i=0}^{9} a_i x^i(t_j)\,, \tag{6.15}$$

with

$$x\left(t_j\right) = 2\frac{t_j - t_s}{t_e - t_s}\,. \tag{6.16}$$

Here t_j is the time stamp at which the correction have to be computed, t_s the start time t_e the stop time of the interval for which the polynomial is defined. Using the speed of light c the ionospheric correction f_{ion}^S scaled to a 2.3 GHz f_S frequency at time t_j can be computed from

$$f_{ion}^S\left(t_j\right) = \frac{f_S}{c} \cdot \frac{\Delta\rho_{ion}\left(t_j + \Delta t\right) - \Delta\rho_{ion}\left(t_j - \Delta t\right)}{\Delta t}. \tag{6.17}$$

This is only true for one-way S-band downlink. Appendix A.5.1 contains formulations from which the correction can be computed for other up- and downlink configurations.

6.3.2 The Klobuchar model

Klobuchar [1975] developed a model by representing the average monthly diurnal behavior of time delay at a location on Earth as a simple positive cosine wave dependence with a constant offset term (see also *Parkinson and Spilker* [1996]):

$$\Delta t_{iono} = \begin{cases} C & \text{if } \frac{(t-\phi)2\pi}{P} > 90\,^\circ \\ C + A\cos\frac{2\pi(t-\phi)}{P} & \text{else.} \end{cases} \tag{6.18}$$

Here, C is the constant offset, A the amplitude, P the period, ϕ the phase of the function and t the local time at the ionospheric point. Using the first two terms of the Taylor expansion of the cosine function:

$$\Delta t_{iono} = C + A\left(1 - \frac{x^2}{2} - \frac{x^4}{24}\right) \qquad \text{with } x = \frac{2\pi\left(t-\phi\right)}{P}\,. \tag{6.19}$$

At the mean ionospheric height of 350 km the zenith angle $z = \sin^{-1}\left(0.94798\cos\epsilon\right)$, where ϵ is the unrefracted auxiliary elevation angle and the numerical $0.94798 = a_e/\left(a_e + 350km\right)$ with $a_e = 6378.136$ km as the mean equatorial radius of the Earth. The geodetic latitude ϕ_I and longitude λ_I of the sub-ionospheric point is computed using the auxiliary azimuth angle σ and the longitude λ_0 of the receiving ground station

$$\phi_I = \sin^{-1}\left(\sin\phi_0\sin\left(\epsilon + z\right) + \cos\phi_0\cos\left(\epsilon + z\right)\cos\sigma\right) \tag{6.20}$$

$$\lambda_I = \lambda_0 + \sin^{-1}\left(\frac{\cos\left(\epsilon + z\right)\sin\sigma}{\cos\phi_I}\right)\,. \tag{6.21}$$

As ionospheric properties are aligned with geomagnetic latitude rather than geographic latitude, the Klobuchar model is formulated in geomagnetic coordinates. The transformation from geodetic to geomagnetic latitude, assuming that the Earth's magnetic field can be represented by an Earth centered dipole, can be achieved by the following approximation (*Klobuchar* [1975]):

$$\Phi_I = \phi_I + 11.6^{\circ} \cos\left(\lambda_I - 291^{\circ}\right) . \tag{6.22}$$

The amplitude A and the period P can be computed from

$$A = A_0 + A_1\Phi_I + A_2\Phi_I^2 + A_3\Phi_I^3 \tag{6.23}$$
$$P = P_0 + P_1\Phi_I + P_2\Phi_I^2 + P_3\Phi_I^3 \tag{6.24}$$

The slant factor is used to convert into slant time and can be approximated by

$$\tau_{sl} = 1 + 2\left(\frac{96 - \epsilon}{90}\right)^3 . \tag{6.25}$$

Thus, the ionospheric path delay in time is (*Klobuchar* [1975])

$$\Delta t_{iono} = \tau_{sl}\left(C + A\left(1 - \frac{x^2}{2} - \frac{x^4}{24}\right)\right) . \tag{6.26}$$

The ranging delay is then

$$\Delta\rho_{iono}(t) = \Delta t_{iono} \cdot c . \tag{6.27}$$

The coefficients A_0, A_1, A_2, A_3 of the amplitude A and P_0, P_1, P_2, P_3 of the period P are available from ftp://ftp.unibe.ch/aiub/CODE/ and are computed from daily measured global ionosphere maps (*Schaer S.* [1997]).

6.3.3 Comparison

In Figure 6.2 the frequency shifts for a two-way X-band downlink computed from the polynomial representation of the path delay provided by the TSAC group and from the Klobuchar model based on an ionospheric map for 1 March 2006 are shown. Obviously both corrections are in good agreement and can be used equivalently.

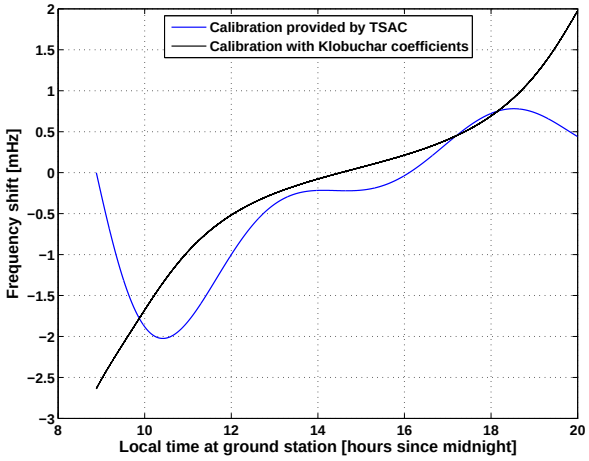

Figure 6.2: *Comparison of the frequency shift for a two-way X-band downlink computed based on Klobuchar coefficients and ionospheric calibration files provided by TSAC for 1 March 2006*

6.4 Frequency shift caused by the atmosphere of the Earth

The total frequency shift depending on the uplink frequency f_{up} and the transponder ratio k for a two-way recording can be computed according to *Pätzold* [2004] via:

$$\Delta f_{cal}(t) = f_{up}(t) \cdot \frac{1+k}{c} \cdot (\Delta\tau_{trop}(t) + \Delta\tau_{iono}(t)) \tag{6.28}$$

where

$$\Delta\tau_{trop}(t) = \frac{\phi_{trop}(t+\Delta t) - \phi_{trop}(t-\Delta t)}{\Delta t} \tag{6.29}$$

$$\Delta\tau_{iono}(t) = \frac{\phi_{iono}(t+\Delta t) - \phi_{iono}(t-\Delta t)}{\Delta t} \tag{6.30}$$

In this equation it is assumed that the elevation angle at the time, when the signal is transmitted from the ground station and when the signal is received at ground station equals. This is only true when the spacecraft is close to the ground station. However, for spacecraft like Rosetta (ROS) this is not true because of the large round trip light time t_τ. Therefore, a formulation should be used in which the elevation angle at transmission and reception is treated separately

$$\begin{aligned}\Delta f_{cal}(t) = {} & f_{up}(t)\frac{k}{c}(\Delta\tau_{trop}(t) + \Delta\tau_{trop}(t-t_\tau) \\ & +\Delta\tau_{iono}(t) + \Delta\tau_{iono}(t-t_\tau)).\end{aligned} \tag{6.31}$$

In Figure 6.3 a comparison of the total frequency shift caused by the atmosphere of the Earth is shown firstly based on equation 6.28 and secondly on equation 6.31 for a measurement in X-band (8.4 GHz) for the ROS spacecraft on 5 September 2009. At the beginning of the recording (small elevation angles) a large difference between the corrections according to equations (6.28) and (6.31) can be seen. It decreases during the recording due to larger elevation angles which reduces the tropospheric correction. For higher accuracy equation (6.31) is used for the computation of the atmospheric correction.

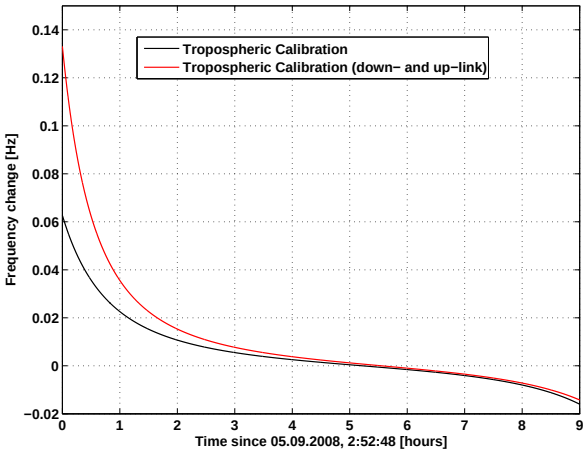

Figure 6.3: *Comparison of the frequency correction for the atmosphere of the Earth in X-band (8.4 GHz) for the Rosetta spacecraft on 5 September 2009. The red line indicates the correction based on the more precise formulation according to equation* (6.31) *and the black line the correction based on a simplified model according to equation* (6.28)

CHAPTER 7

Orbit determination and parameter estimation

The equation of motion of a spacecraft contains parameter which need to be estimated from the measured data. For example, the initial state vector of the spacecraft, the scale factor for the solar radiation pressure or the core parameter of this thesis, the mass, and if possible other parameter of the gravity field of a body. This can be realized by a weighted least square estimation method. Applying this method means dealing with the inverse of matrix which may be ill-posed or contain unimportant parameter. The least square fitting method and numerical solutions for the problems are described in the following.

7.1 Weighted least squares estimation

The basic idea of least square estimation is to find the model parameter for which the square of the difference between the model data and the measured data becomes as small as possible. Assuming a vector consisting of m recorded data

$$\boldsymbol{d} = (d_1, d_2, ..., d_m)^T$$

and a vector

$$\boldsymbol{x} = (x_1, x_2, ..., x_n)^T$$

containing n free model parameters like the mass of the body. The model $\boldsymbol{g}$ provides a link between the model parameters and observations:

$$\boldsymbol{g}(\boldsymbol{x}) = (g_1(\boldsymbol{x}), g_2(\boldsymbol{x}), ..., g_m(\boldsymbol{x}))^T .$$

Here, $g_i(\boldsymbol{x})$ is the value predicted by the model for observation d_i. The difference between the model data and the observation is then

$$\boldsymbol{\epsilon} = \boldsymbol{d} - \boldsymbol{g}. \tag{7.1}$$

In order to compute values of $\boldsymbol{x}$ such that $\boldsymbol{g}(\boldsymbol{x})$ matches $\boldsymbol{d}$, the partial derivatives of the model $\boldsymbol{g}$ is expanded around $\boldsymbol{x}$ in a Taylor series

$$\boldsymbol{g}(\boldsymbol{x} + \delta\boldsymbol{x}) = \boldsymbol{g}(\boldsymbol{x}) + \boldsymbol{J}\delta\boldsymbol{x} + \boldsymbol{R}(\boldsymbol{g}, \delta\boldsymbol{x}) . \tag{7.2}$$

If the model function $\boldsymbol{g}$ is linear it can be written as

$$\boldsymbol{g}(\boldsymbol{x} + \delta\boldsymbol{x}) = \boldsymbol{g}(\boldsymbol{x}) + \boldsymbol{J}\delta\boldsymbol{x} . \tag{7.3}$$

$\boldsymbol{J}$ is the $(m \times n)$ Jacobian matrix also referred to as sensitivity matrix containing the partial derivatives of the model function

$$\boldsymbol{J} = \begin{pmatrix} \frac{\partial g_1}{\partial x_1} & \cdots & \frac{\partial g_m}{\partial x_1} \\ \vdots & \ddots & \vdots \\ \frac{\partial g_1}{\partial x_n} & \cdots & \frac{\partial g_m}{\partial x_n} \end{pmatrix} \qquad (1 \leq i \leq m, 1 \leq j \leq n)$$

The partial derivatives in $\boldsymbol{J}$ can be derived analytically for each parameter if an appropriate analytical function is available. The analytical expression of the partial derivatives can become very complex and the numerical implementation of the corresponding formulas is quite laborious and error prone. The rigorous computation can be replaced by a simple difference quotient approximation. With a symmetric differential quotient approximation

$$\frac{\partial g_i}{\partial x_j} = \frac{g\left(x_j + \Delta x_j\right) - g\left(x_j - \Delta x_j\right)}{2\Delta x_j}. \tag{7.4}$$

the partial derivatives are obtained which are correct up to second order in x_j (*Montenbruck and Gill* [2000]).

So far, all observations are treated equally, but the noise of measurements usually varies, i.e. the standard deviation σ_i is different. This difference can be accounted for by introducing an $(m \times m)$ weight matrix (*Juup and Vozoff* [1975])

$$\boldsymbol{W} = diag\left(\sigma_1^{-2}, \sigma_2^{-2}, ..., \sigma_m^{-2}\right) = \begin{pmatrix} \sigma_1^{-2} & & 0 \\ & \ddots & \\ 0 & & \sigma_m^{-2} \end{pmatrix}. \tag{7.5}$$

Agreement between the measured data and the model data with respect to the model parameter can be found by minimizing

$$\begin{aligned} \boldsymbol{q}(\boldsymbol{x}) &= ||\boldsymbol{\epsilon} - \boldsymbol{J}\delta\boldsymbol{x}||_{\boldsymbol{W}} = \\ &= \left(\left(\boldsymbol{d} - \boldsymbol{g}(\boldsymbol{x}) - \boldsymbol{J}\delta\boldsymbol{x}\right)^T \boldsymbol{W}\left(\boldsymbol{d} - \boldsymbol{g}(\boldsymbol{x}) - \boldsymbol{J}\delta\boldsymbol{x}\right)\right)^{\frac{1}{2}} \qquad (7.6) \\ \Rightarrow \boldsymbol{q}^2(\boldsymbol{x}) &= \boldsymbol{\epsilon}^T\boldsymbol{W}\boldsymbol{\epsilon} - 2\boldsymbol{J}^T\boldsymbol{W}\boldsymbol{\epsilon}\delta\boldsymbol{x} + \boldsymbol{J}^T\boldsymbol{W}\boldsymbol{J}\delta^2\boldsymbol{x}\,. \qquad (7.7) \end{aligned}$$

Differentiation with respect to $\boldsymbol{x}$ leads to

$$\delta\boldsymbol{x} = \left(\boldsymbol{J}^T\boldsymbol{W}\boldsymbol{J}\right)^{-1}\boldsymbol{J}^T\boldsymbol{W}\boldsymbol{\epsilon}. \tag{7.8}$$

This formulation can be used to estimate in an iterative process a new model with new parameter from the change $\delta\boldsymbol{x}$ in order to minimize the difference between measured data and model data (*Juup and Vozoff* [1975], *Aster et al.* [2005]).

7.2 Singular value decomposition

The inverse of the matrix $\left(\boldsymbol{J}^T\boldsymbol{W}\boldsymbol{J}\right)$ in equation 7.8 can be computed numerically using Singular Value Decomposition (SVD). The SVD for an $(m \times n)$ matrix $\boldsymbol{A}$ with rank $p \leq \min(m, n)$ is denoted by

$$\boldsymbol{A} = \boldsymbol{U}\boldsymbol{S}\boldsymbol{V}^T = \sum_{i=1}^{n} s_i \boldsymbol{u}_i \boldsymbol{v}_i^T \,, \tag{7.9}$$

where $\boldsymbol{U}$ is an $(m \times m)$ and $\boldsymbol{V}$ an $(n \times n)$ matrix. $\boldsymbol{U}$ and $\boldsymbol{V}$ are orthogonal matrices

$$\boldsymbol{U}^T\boldsymbol{U} = \boldsymbol{I}_m \tag{7.10}$$

$$\boldsymbol{V}^T\boldsymbol{V} = \boldsymbol{I}_n \,. \tag{7.11}$$

$\boldsymbol{S}$ is an $(m \times n)$ diagonal matrix where each diagonal element s_i is the non-negative square root of an eigenvalue of $\boldsymbol{A}^T\boldsymbol{A}$. The pseudo inverse of $\boldsymbol{A}$ can now be computed via

$$\boldsymbol{A}^{-1} = \boldsymbol{V}\boldsymbol{S}^{-1}\boldsymbol{U}^T = \sum_{i=1}^{n} \frac{\boldsymbol{v}_i \boldsymbol{u}_i^T}{s_i} \,, \tag{7.12}$$

with the so called singular values s_i

$$s_i^{-1} = \begin{cases} \frac{1}{s_i} & \text{if } s_i > 0 \\ 0 & \text{if } s_i = 0. \end{cases} \tag{7.13}$$

For numerical purposes this formulation is not appropriate because s_i will not be exactly zero and therefore the inversion will be instable. Additionally very small values of s_i would produce very large values of s_i^{-1}. For this reason the change of the respective parameter would be overestimated and result in wrong parameter estimation or divergence of the iteration process. A method to solve this problem will be explained in the next section.

7.3 Damping factor

The numerical values of s_i can lead to ill-posedness through irrelevant parameter (zero singular values of $\boldsymbol{A}$), and unimportant parameters (small singular values of $\boldsymbol{A}$). One way would be to omit terms with small singular values. This would stabilize the solution in the sense that it would make the result less sensitive to data noise. But this would also reduce the resolution and the model estimation would no longer be unbiased.

The problem can be solved by introducing a damping factor α. Equation 7.8 becomes then

$$\delta\boldsymbol{x} = \left(\boldsymbol{J}^T\boldsymbol{W}\boldsymbol{J} + \alpha^2\boldsymbol{I}\right)^{-1}\boldsymbol{J}^T\boldsymbol{W}\boldsymbol{\epsilon}. \tag{7.14}$$

The damping factor α can be obtained from the Eigenvalues of the Jacobian matrix $\boldsymbol{J}$ according to *Aster et al.* [2005] via

$$\alpha = max\left(eig\left(\left(\boldsymbol{J}^T\boldsymbol{W}\right)^{-1}\right)\right) .$$

This numerical method provides a stable weighted least square estimation algorithm which can be used to determine the parameter of a model to be fitted to recorded data within an iterative process.

7.4 Error estimation

The recordings from Radio Science measurements are affected by measurement errors. These errors influence the uncertainty of the estimated parameter. The covariance matrix $\boldsymbol{P}$ contains the estimates for the closeness of the model with the measurement data and is defined as (*Vallado* [2001])

$$\boldsymbol{P} = \left(\boldsymbol{J}^T\boldsymbol{W}\boldsymbol{J}\right)^{-1} = \begin{pmatrix} \sigma_{11}^2 & \cdots & \mu_{1\,i}\sigma_1\sigma_i & \cdots & \mu_{1\,n}\sigma_1\sigma_n \\ \vdots & \ddots & & & \vdots \\ \mu_{i\,1}\sigma_i\sigma_1 & & \sigma_{ii}^2 & & \mu_{i\,n}\sigma_i\sigma_n \\ \vdots & & & \ddots & \vdots \\ \mu_{n\,1}\sigma_n\sigma_1 & \cdots & \mu_{n\,i}\sigma_n\sigma_i & \cdots & \sigma_{nn}^2 \end{pmatrix} \tag{7.15}$$

with the Jacobian matrix $\boldsymbol{J}$ and the weight matrix $\boldsymbol{W}$ as defined above. The diagonal terms are the variances σ_{ii}^2 of the estimate and the square root of the variances are the sample standard deviations σ_{ii} of each estimated parameter. The 95% confidence interval, i.e. 1 σ of the parameter x_i is (*Aster et al.* [2005])

$$\Delta x_i = \pm 1.96 \cdot \sqrt{\boldsymbol{P}_{ii}} \tag{7.16}$$

The factor 1.96 results from

$$\frac{1}{\sigma\sqrt{2\pi}} \int_{-1.96\sigma}^{1.96\sigma} e^{-\frac{x^2}{2\sigma^2}} dx \approx 0.95 . \tag{7.17}$$

The off-diagonal elements of $\boldsymbol{P}$ are called covariance terms. They contain the correlation coefficients $\mu_{i\,j}$ representing the degree of correlation among the estimated parameter. Zero indicates no correlation, positive signs a direct correlation, while negative signs imply an inverse relationship. The correlation should be zero or, at least, very small (*Brandt* [1998], *Montenbruck and Gill* [2000]).

CHAPTER 8

Noise reduction filter

The uncertainty in the parameter estimated from the recored data increases with the noise of the data. Applying digital filters can be used to reduce the noise. In the following only a brief introduction into digital filter is given, a detailed description would go beyond the scope of this work. In addition, the filters which are used in this work and the method for selection of the filter are explained.

8.1 Noise sources

The noise of the data recorded at the ground station is generated mostly by the following sources (*Pätzold et al.* [2004]):

- Thermal noise essentially by the receiver of the ground station, but also from the transponder onboard the spacecraft.
- Instrumentation errors like quantization errors or reference instability.
- The troposphere and ionosphere of the Earth, and the interplanetary plasma. These contributions are modeled and subtracted from the recorded data, but not all contributions can be removed entirely (see section 6).

The velocity error σ_v due to the thermal noise of the receiver at the ground station is given by

$$\sigma_v = \frac{c}{4\pi f \Delta t}\sqrt{\frac{2BN_0}{C}} \tag{8.1}$$

and the phase noise σ_ϕ of the transponder by (*Pätzold et al.* [2004])

$$\sigma_\phi = \frac{c\sqrt{2}}{4\pi f t}\sigma_v \,. \tag{8.2}$$

c is the speed of light, f the frequency, Δt the sample time, B the receiver bandwidth, C and N the received carrier power and the noise power density, respectively. The transponder phase noise σ_ϕ was experimentally determined by *Remus et al.* [2001] for Mars Express and Rosetta with a transponder electrical qualification model on ground. A summary of the Doppler velocity errors at different distances is given in Table 8.1. The total error in X-band in two-way coherent mode of 0.26 mm/s corresponds to an error of 14.6 mHz referring to a downlink frequency of 8.4 GHz.

More information about noise sources during Radio Science measurements is given in *Yuen* [1983] and more detailed information for MEX and ROS can be found in *Pätzold* [2003], and *Pätzold* [2006], respectively.

	at 0.8 AU		at 2.5 AU	
	S-Band	**X-Band**	**S-Band**	**X-Band**
Thermal noise (ground station) [mm/s]	0.90	0.01	2.00	0.03
Transponder phase noise [mm/s]	0.42	0.26	0.42	0.26
Total error [mm/s]	0.99	0.26	2.04	0.26

Table 8.1: *The Doppler velocity error in two-way coherent mode at different distances for Mars Express and Rosetta at 1 sec integration time (Pätzold et al. [2004]).*

8.2 Digital filters

The noise of a measurement can be reduced by applying filter. In general, a filter can be considered as a transfer function between any input function $x(t)$ and the according output function $y(t)$. Here, digital filters are used, i.e. filtering is applied numerically. The discrete input sequence

$$x(t) = x_n = x\,(n\Delta t) \qquad n = 0, 1, 2, ..., N-1\,, \tag{8.3}$$

with a time interval Δt and N samples is related to the output sequence y_n in the time domain via the discrete convolution

$$y(t) = y_n = \sum_{j=0}^{N-1} h_j x_{n-j}\,. \tag{8.4}$$

In the time domain, digital filters are characterized by the discrete impulse response function h_n and in the frequency domain by its discrete Fourier transformation, the discrete frequency response function H_k. The input to output relation is according to the convolution theorem in the frequency domain

$$Y_k = H_k X_k\,. \tag{8.5}$$

The discrete input function $x(t)$ is in the frequency domain using the discrete Fourier transformation

$$X(f) = X(\Delta f k) = X_k = \Delta t \sum_{n=0}^{N-1} x_n e^{-i2\pi k \Delta f n \Delta t}\,, \tag{8.6}$$

were the frequency $f = k\Delta f$ and the sample frequency $\Delta f = \frac{1}{T} = \frac{1}{N\Delta t}$. Replacing f with the new variable (*Häusler* [2008*a*])

$$z = e^{-i2\pi k \Delta f \Delta t} \tag{8.7}$$

results in the z-transform of the discrete input function

$$\mathcal{Z}\,(x_n) = X(z) = \Delta t \sum_{n=0}^{N-1} x_n z^n\,. \tag{8.8}$$

The sum on the right side is the z-transform of $x(t)$. The discrete convolution of two sequences can be realized by the product of their z-transforms (*Buttkus* [2000]). Therefore equation (8.5) reads then in the z domain

$$Y(z) = H(z)X(z)\,. \tag{8.9}$$

The most important class of digital filters are filters where the transfer function $H(z)$ can be written as the ratio of two polynomials in z:

$$H(z) = \frac{\sum\limits_{k=k_0}^{M} a_k z^k}{\sum\limits_{k=0}^{L} b_k z^k}, \qquad \text{with } b_0 = 1\,. \tag{8.10}$$

It follows from the input to output relation (8.9) in the z domain

$$\begin{aligned} &\left(1 + b_1 z + b_2 z^2 + ... + b_L z^L\right) Y(z) = \\ &\left(a_{k_0} z^{k_0} + a_{k_0+1} z^{k_0+1} + ... + a_M z^M\right) X(z)\,. \end{aligned} \tag{8.11}$$

Using that $X(z)z^k$ is the z transform of the time series (x_{j-k}) it can be transformed to

$$\begin{aligned} &(y_n) + b_1(y_{n-1}) + ... + b_L(y_{n-L}) = \\ &a_{k_0}\,(x_{n-k_0}) + a_{k_0+1}\,(x_{n-k_0-1}) + ... + a_M\,(x_{n-M})\,. \end{aligned} \tag{8.12}$$

Therefore the following recursive filter equation is fulfilled at any time n

$$\begin{aligned} y_n \;=\; & a_{k_0}\,(x_{n-k_0}) + a_{k_0+1}\,(x_{n-k_0-1}) + ... + a_M\,(x_{n-M}) \\ & -b_1(y_{n-1}) - ... - b_L(y_{n-L}). \end{aligned} \tag{8.13}$$

The filter can be classified with regard to the coefficients b_k in equation (8.10). For nonrecursive filters of finite length all b_k are all equal to zero for $k \geq 1$. $H(z)$ is then a polynomial with zeroes, but without poles. If one of the coefficients b_k is not equal to zero for $k \neq 0$, the filter is recursive (*Buttkus* [2000]).

Filters can also be distinguished by their phase response into Zero phase filters having a frequency response that has a phase which is composed entirely of zeroes, and the frequency response of linear phase filters and nonlinear phase filters having linear and nonlinear phases, respectively. Zero phase can be achieved by combining forward and reverse filtering, i.e after filtering in the forward direction, then filtering again in the reverse direction. The result has then a frequency response with zero phase (*Smith* [1998]).

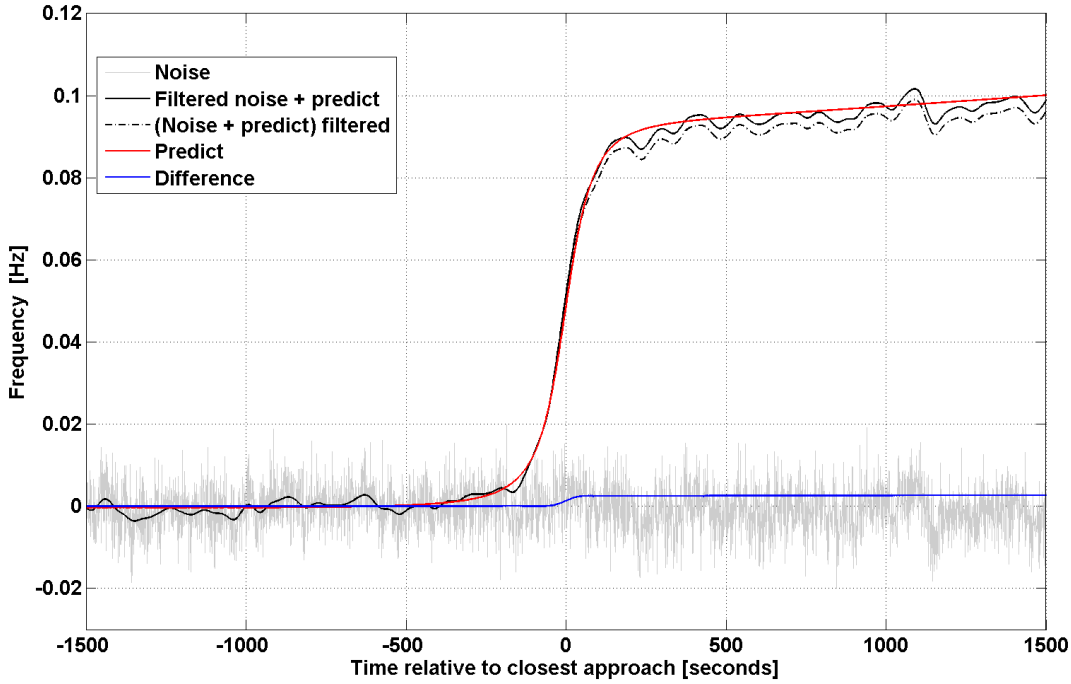

(a) Kaiser window filtering with cut-off frequency $f_c = 15$ mHz

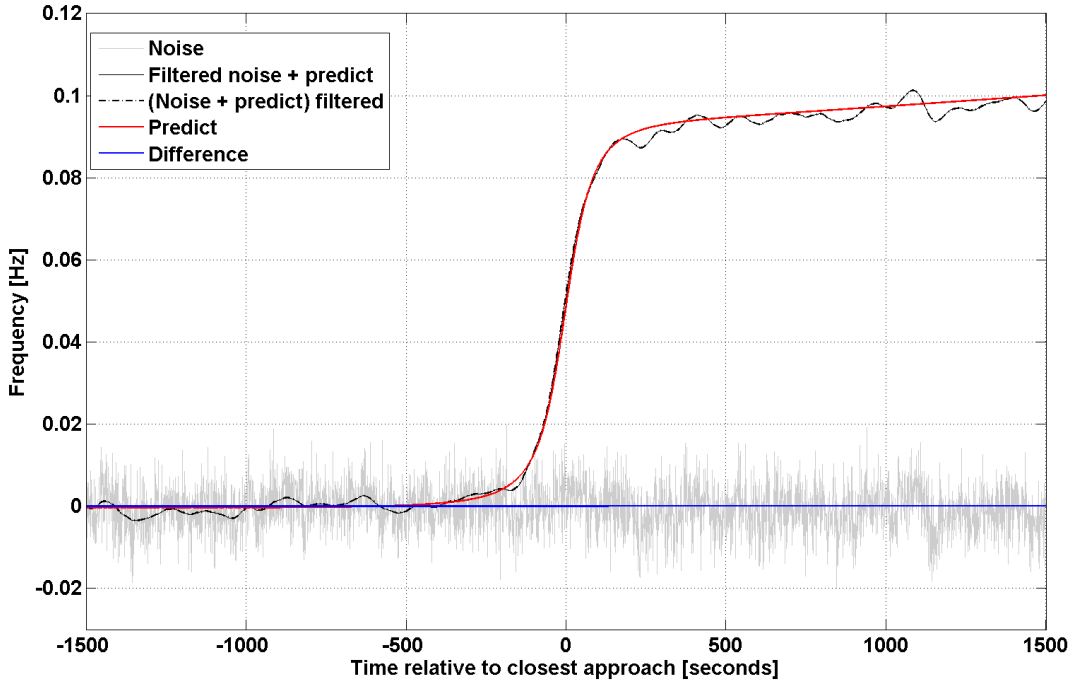

(b) Kaiser window filtering with cut-off frequency $f_c = 47$ mHz

Figure 8.1: *Comparison of applied filters. The used data are from the Phobos flyby in July, 2008. Here different cut-off frequencies for the Kaiser window are used. In the figure above the filter reduces not only the noise but also the frequency shift caused by the gravity field of Phobos, indicated by the blue line, i.e. the difference between f_n and the filtered noise $\check{f}_n$. In the figure below only the noise is reduced because $\left|f_n - \check{f}_n\right|$ is approximately zero.*

8.3 Appropriate filter

Not all digital filters are useful for every type of measurement. The filter with its specific configuration parameter should reduce only the noise of the data and leave the frequency change caused by the gravity field of the perturbing body unmodified. This frequency change is different for every measurement. For this reason the parameter of the selected filter has to be defined for each measurement separately.

Stiffel [2008] tested different filters in order to find the best filter with specific configuration parameters for each performed flyby. Hence predicted frequency changes f_p are generated and real noise f_n from a measurement is added. The filter is then applied to the noisy predicted frequency changes $f_{pn} = f_p + f_n$ and in addition to the noise f_n only. Subtracting from the filtered noisy predicted frequency changes the predicted frequency changes only filtered noise f_n remains. The difference between f_n and the filtered noise $\check{f}_n$ indicates the quality of the filter. Defining a limit f_l according to the measurement accuracy, the filter reduces only the noise if $\left|f_n - \check{f}_n\right|$ is smaller than f_l. If $\left|f_n - \check{f}_n\right|$ is larger than f_l, the filter reduces the noise but changes also the frequency shift caused by the gravitational attraction of the perturbing body, i.e.

$$\Big|\underbrace{filt\left(f_{pn}\right) - f_p}_{f_n} - \underbrace{filt\left(f_n\right)}_{\check{f}_n}\Big| \begin{cases} < f_l & \Rightarrow \text{only noise reduced} \\ \geq f_l & \Rightarrow f_p \text{ also modified.} \end{cases} \tag{8.14}$$

Figure 8.1 shows two examples for the result of the above described method. The applied filter was a Kaiser window with two different cut-off frequencies f_c. The cut-off frequency defines the bandwidth of the filter. In Figure 8.1(a) the selected cut-off frequency of 15 mHz seems to be too small and not only noise is reduced but also the frequency change caused by the perturbing body is modified. The resulting mass estimate would be falsified. In Figure 8.1(b) the ideal cut-off frequency is selected which can be seen by the nearly zero difference (indicated by the blue line) between $\check{f}_n$ and f_n.

Stiffel [2008] found out with this method that a Kaiser window filter and a moving average filter applied consecutively reducing most of the measurement noise.

The Kaiser window filter is defined (*Buttkus* [2000])

$$w(k) = \begin{cases} \frac{I_0\left(\alpha\sqrt{1-\frac{2k}{(N-1)^2}}\right)}{I_0(\alpha)} & \text{if } |k| \leq \frac{N-1}{2} \\ 0 & \text{if } |k| > \frac{N-1}{2}, \end{cases} \tag{8.15}$$

with N the number of data points, $k = 1, 2 \ldots N$, and the Bessel function $I_0(\alpha)$ of zeroth order

$$I_0(\alpha) = 1 + \sum_{k=1}^{\infty} \left(\frac{\left(\frac{\alpha}{2}\right)^2}{k!} \right)^2 . \tag{8.16}$$

The parameter α changes the amplitude of the side lobes and the transition bandwidth.

The moving average filter is defined by

$$y(n) = \frac{1}{M} \sum_{k=0}^{M-1} x(n-k), \tag{8.17}$$

with n the current time at which the value should be calculated and M the length of the time interval used for averaging (*Buttkus* [2000]).

For the analysis of the measured data from close flybys only these two filters are used. Both filters are applied consecutively in forward and reverse direction ensuring a zero phase.

The limit f_l needed to define the cut-off frequency f_c of the Kaiser window filter and the time interval M of the moving average filter is computed from the sensitivity GM_s. The sensitivity is estimated from an upper and lower limit of the mass value and the resulting upper and lower limit of the amplitude of the frequency change caused by the gravitational attraction of the mass, i.e.

$$GM_s = \frac{GM_{up} - GM_{low}}{f_{up} - f_{low}} = \frac{\Delta GM}{\Delta f} \tag{8.18}$$

This method ensures that the used filter technique only reduces the noise level and does not eliminate any information about the mass of the body in the measured data. Applying these filters with a priori estimated configuration parameters decreases the standard deviation of the measurement noise at least by a factor of 3 (*Stiffel* [2008]).

APPENDIX A

Appendix

A.1 Parameter

A.1.1 ROS

The optical parameter of ROS are listed in the following table based on information from *Morley* [2008], whereby $ABSC$ is the absorption coefficient, $DIFR$ the ratio diffusive/(diffusive + specular) with (diffusive + specular) = 1 - ABSC and the reflection coefficient ε.

Surface	α	δ	ε	**Area [m²]**
+ X	0.909	0.091	0.000	5.150
- X	0.853	0.136	0.011	5.150
+ Y	0.795	0.205	0.000	5.408
- Y	0.750	0.250	0.000	5.408
+ Z	0.916	0.084	0.000	4.200
- Z	0.889	0.080	0.031	4.200
HGA	0.930	0.070	0.000	3.800
solar array	0.840	0.313	0.110	32.310

Table A.1: *Optical properties of the ROS spacecraft from Morley [2008]*

A.2 Tectonic plate motion

Plate Name	Ω_x **[rad/My.]**	Ω_y **[rad/My.]**	Ω_z **[rad/My.]**
Pacific	-0.001510	0.004840	-0.009970
Cocos	-0.010425	-0.021605	0.010925
Nazca	-0.001532	-0.008577	0.009609
Caribbean	-0.000178	-0.003385	0.001581
South America	-0.001038	-0.001515	-0.000870
Antarctica	-0.000821	-0.001701	0.003706
India	0.006670	0.000040	0.006790
Australia	0.007839	0.005124	0.006282
Africa	0.000891	-0.003099	0.003922
Arabia	0.006685	-0.000521	0.006760
Eurasia	-0.000981	-0.002395	0.003153
North America	0.000258	-0.003599	-0.000153
Juan de Fuca	0.005200	0.008610	-0.005820
Philippine	0.010090	-0.007160	-0.009670
Rivera	-0.009390	-0.030960	0.012050
Scotia	-0.000410	-0.002660	-0.001270

Table A.2: *Cartesian rotation vector for each plate using the NNR-NUVEL1A kinematic plate model (no net rotation) (IERS [2009])*

A.3 Coefficient tableau of integration method

0	0	0	0	0	0	0	0
$\frac{1}{5}$	$\frac{1}{5}$	0	0	0	0	0	0
$\frac{3}{10}$	$\frac{3}{40}$	$\frac{9}{40}$	0	0	0	0	0
$\frac{4}{5}$	$\frac{44}{45}$	$-\frac{56}{15}$	$\frac{32}{9}$	0	0	0	0
$\frac{8}{9}$	$\frac{19372}{6561}$	$-\frac{25360}{2187}$	$\frac{64448}{6561}$	$-\frac{212}{729}$	0	0	0
1	$\frac{9017}{3168}$	$-\frac{355}{33}$	$\frac{46732}{5247}$	$\frac{49}{176}$	$-\frac{5103}{18656}$	0	0
1	$\frac{35}{384}$	0	$\frac{500}{1113}$	$\frac{125}{192}$	$-\frac{2187}{6784}$	$\frac{11}{84}$	0
0	$\frac{5179}{57600}$	0	$\frac{7571}{16695}$	$\frac{393}{640}$	$-\frac{92097}{339200}$	$\frac{187}{2100}$	$\frac{1}{40}$
0	$\frac{35}{384}$	0	$\frac{500}{1113}$	$\frac{125}{192}$	$-\frac{2187}{6784}$	$\frac{11}{84}$	0

Table A.3: *The coefficient tableau of the RK5(4) integration method*

.

A.4 Acceleration from unnormalized gravity coefficients

In the following the equations in order to compute the acceleration caused by the gravity potential of body using unormalized gravity coefficients $C_{n,\,m}$ and $S_{n,\,m}$ according to *Montenbruck and Gill* [2000] are shown.

A.4.1 Recursions

The unnomralized recurence coefficients $V_{n,\,m}$ and $W_{n,\,m}$ can be computed according to *Montenbruck and Gill* [2000]

$$V_{m,\,m} = \frac{\overline{R}}{r^2} \cdot (2m-1)\,(x \cdot V_{m-1,\,m-1} - y \cdot W_{m-1,\,m-1}) \tag{A.1a}$$

$$W_{m,\,m} = \frac{\overline{R}}{r^2} \cdot (2m-1)\,(x \cdot W_{m-1,\,m-1} + y \cdot V_{m-1,\,m-1}) \tag{A.1b}$$

$$V_{n,\,m} = \frac{\overline{R}}{r^2} \cdot \frac{1}{n-m}\left((2n-1) \cdot z \cdot V_{n-1,\,m} - (n+m-1) \cdot \overline{R} \cdot V_{n-2,\,m}\right) \tag{A.1c}$$

$$W_{n,\,m} = \frac{\overline{R}}{r^2} \cdot \frac{1}{n-m}\left((2n-1) \cdot z \cdot W_{n-1,\,m} - (n+m-1) \cdot \overline{R} \cdot W_{n-2,\,m}\right) \tag{A.1d}$$

with the initial conditions

$$V_{0,\,0} = \frac{\overline{R}}{r} \quad \text{and} \quad W_{0,\,0} = 0 \tag{A.2}$$

In order to compute the all $V_{n,\,m}$ and $W_{n,\,m}$ the zonal terms have to be computed first and all further computations should be done according to the scheme shown in figure A.1.

A.4.2 Acceleration

With the above shown unnormalized recurrence coefficients the resulting acceleration can be computed via the following equation using unnormalized gravity coefficients $C_{n,\,m}$ and $S_{n,\,m}$.

$$\ddot{x} = \sum_{n=0}^{\infty}\sum_{m=0}^{n} \ddot{x}_{n,m}\ , \qquad \ddot{y} = \sum_{n=0}^{\infty}\sum_{m=0}^{n} \ddot{y}_{n,m}\ , \qquad \ddot{z} = \sum_{n=0}^{\infty}\sum_{m=0}^{n} \ddot{z}_{n,m} \tag{A.3}$$

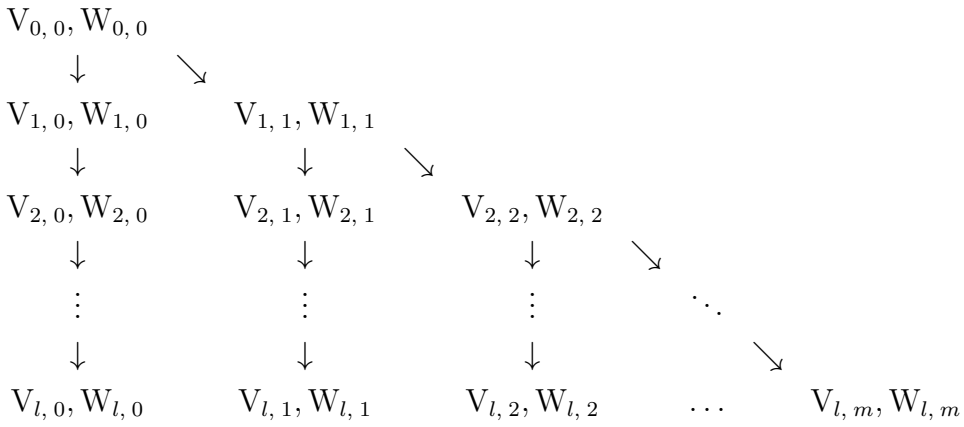

Figure A.1: *Execution scheme for recurrence coefficients computation.*

The parital accelerations are (see *Montenbruck and Gill* [2000])

$$\ddot{x}_{n,m} = -\frac{GM}{\overline{R}^2} \cdot C_{n,0} \cdot V_{n+1,1} \tag{A.4}$$

$$\begin{aligned} \ddot{x}_{n,m} \overset{m>0}{=} & -\frac{1}{2}\frac{GM}{\overline{R}^2}\Big(C_{n,m} \cdot V_{n+1,m+1} + S_{n,m} \cdot W_{n+1,m+1} \\ & - (n-m+2)(n-m+1)\Big(C_{n,m} \cdot V_{n+1,m-1} + \\ & + S_{n,m} \cdot W_{n+1,m-1}\Big)\Big) \end{aligned} \tag{A.5}$$

$$\ddot{y}_{n,m} = -\frac{GM}{\overline{R}^2} \cdot C_{n,0} \cdot W_{n+1,1} \tag{A.6}$$

$$\begin{aligned} \ddot{y}_{n,m} \overset{m>0}{=} & -\frac{1}{2}\frac{GM}{\overline{R}^2}\Big(C_{n,m} \cdot W_{n+1,m+1} - S_{n,m} \cdot V_{n+1,m+1} \\ & + (n-m+2)(n-m+1)\Big(C_{n,m} \cdot W_{n+1,m-1} - \\ & - S_{n,m} \cdot V_{n+1,m-1}\Big)\Big) \end{aligned} \tag{A.7}$$

$$\ddot{z}_{n,0} = -\frac{GM}{\overline{R}^2}(n+1) \cdot C_{n,0} \cdot V_{n+1,0} \tag{A.8}$$

$$\ddot{z}_{n,m} \overset{m>0}{=} -\frac{GM}{\overline{R}^2}(n-m+1) \cdot (C_{n,m} \cdot V_{n+1,m} + S_{n,m} \cdot W_{n+1,m}). \tag{A.9}$$

A.5 Media correction

A.5.1 Ionospheric media correction terms

With the following equations the corrected frequency residuals from the ionospheric correction can be computed for different down- and uplink configurations (*Morabito and Asmar* [1995]):

- One-way S-band downlink (2.3 GHz):

$$\Delta f_c^S(t_j) = \Delta f^S(t_j) - f_{ion}^S(t_j) \tag{A.10}$$

- One-way S-band downlink (2.3 GHz):

$$\Delta f_c^X(t_j) = \Delta f^X(t_j) - \frac{3}{11} f_{ion}^S(t_j) \tag{A.11}$$

- Two-way X-band uplink and X-band downlink:

$$\Delta f_c^X(t_j) = \Delta f^X(t_j) - \frac{3}{11}\left(f_{ion}^S(t_j) - \frac{840}{749} f_{ion}^S(t_j - t_r)\right) \tag{A.12}$$

- Two-way X-band uplink and S-band downlink:

$$\Delta f_c^X(t_j) = \Delta f^X(t_j) - f_{ion}^S(t_j) - \frac{3}{11}\frac{840}{749} f_{ion}^S(t_j - t_r) \tag{A.13}$$

Here t_r is the two-way light time. In the equations for the two-way correction the first term accounts for the downlink and the second one accounts for the uplink and the effect of the uplink onto the downlink signal.

A.5.2 Ionospheric correction using the differential Doppler

The correction of the contribution by the ionosphere of the Earth and the interplanetary plasma can also be computed via the differential Doppler defined as follows:

$$\delta f = f_S - \frac{3}{11} f_X \,. \tag{A.14}$$

The differential Doppler is also

$$\delta f = -\frac{1}{2c}\frac{1}{4\pi^2}\frac{e^2}{m_e \epsilon_0}\left(\frac{1}{f_S^2} - \frac{1}{f_X^2}\right) f_s \frac{dI}{dt} \tag{A.15}$$

and therefore the temporal change of the electron content is

$$\frac{dI}{dt} = -\left(\frac{1}{2c}\frac{1}{4\pi^2}\frac{e^2}{m_e \epsilon_0}\right)^{-1} \frac{\delta f}{f_S}\left(\frac{1}{f_S^2} - \frac{1}{f_X^2}\right)^{-1} \tag{A.16}$$

.

The plasma correction for S-band and X-band are then according to *Pätzold* [2004]:

$$f_{S,calib} = f_S + \frac{1}{2c}\frac{1}{4\pi^2}\frac{e^2}{m_e \epsilon_0}\frac{1}{f_S}\frac{dI}{dt} \tag{A.17}$$

$$f_{X,calib} = f_X + \frac{1}{2c}\frac{1}{4\pi^2}\frac{e^2}{m_e \epsilon_0}\frac{1}{f_X}\frac{dI}{dt} \tag{A.18}$$

Using equation A.16 and the general relation

$$\frac{f_S}{f_X} = \frac{3}{11} \tag{A.19}$$

the calibration can now be written as

$$\Delta f_{X,\,Plasma} = -\delta f \frac{33}{112} \tag{A.20}$$

$$\Delta f_{S,\,Plasma} = -\delta f \frac{121}{112}. \tag{A.21}$$

Bibliography

Abramowitz, M. and I. Stegun, *Handbook of Mathematical Functions*, Dover Publ., 1970.

Agnew, D. C., Earth tides, in *Geodesy*, edited by T. Herring, vol 3 of *Treatise on Geophysics*, 163–195, Elsevier, Amsterdam, 2007.

Ashby, N., Relativity in the Global Positioning System, *Living Reviews in Relativity*, 2003.

Aster, R. C., B. Borchers and C. Thurber, *Parameter Estimation and Inverse Problems*, Elsevier Academic Press, 2005.

Battin, R. H., *An Introduction to the Mathematics and Methods of Astrodynamics*, American Institute of Aeronautics and Astronautics, Inc., 3. Auflage, 1987.

Brandt, S., *Data Analysis*, Springer-Verlag, New York, Berlin, Heidelberg, 3. Auflage, 1998.

Buttkus, B., *Spectral analysis and filter theory in applied geophysics*, Springer Verlag, Berlin, Heidelberg, 1. Auflage, 2000.

Chao, C. C., A Model for Tropospheric Calibration from Daily Surface and Radiosonde Balloon Measurements, *Technical Memorandum 391-350*, 1972.

Cunningham, L. E., On the Computation of the Spherical Harmonic Terms Needed during the Numerical Integration of the Orbital Motion of an Artificial Satellite, *Celestial Mechanics*, *2*, 207–216, 1970.

Dehant, V. and P. M. Mathews, Earth rotation variations, in *Geodesy*, edited by T. Herring, vol 3 of *Treatise on Geophysics*, 295–349, Elsevier, Amsterdam, 2007.

Dorfmüller, T. et al., *Lehrbuch der Experimentalphysik, Band 1, Mechanik, Relativität, Wärme*, Walter de Gruyter, Berlin, New York, 11. Auflage, 1998.

Dormand, J. R. and P. J. Prince, A Family of Embedded Runge-Kutta Formulae, *Journal of computational and applied mathematics*, *6*, 19–26, 1980.

Dormand, J. R. and P. J. Prince, High Order Embedded Runge-Kutta Formulae, *Journal of computational and applied mathematics*, *7*, 67–75, 1981.

Gander, W., *Computermathematik*, Birkhäuser Verlag, Basel, 1985.

Gehrke, W., *Fortran 90 Referenzhandbuch*, Carl Hanser Verlag, München, Wien, 1. Auflage, 1991.

Guthmann, A., *Einführung in die Himmelsmechanik und Ephemeridenrechnung*, BI-Wiss.-Verlag, 1994.

Häusler, B., Radio Science Messungen im Sonnensystem mit einer Einführung in die Theorie der Gravitation, *Forschungsbericht*, *LRT-WE-9-FB-2*, 2002.

Häusler, B., Dynamik und Regelung von Satelliten, *Lecture Notes*, 2008*a*.

Häusler, B., Satellitensysteme, *Lecture Notes*, 2008*b*.

Häusler, B., Weltraumphysik, *Lecture Notes*, 2008*c*.

Häusler, B. et al., Venus Express Radio Science Experiment VeRa: Reference Systems and Techniques Used for the Simulation and Prediction of Atmospheric and Ionospheric Sounding Measurements at Planet Venus, *Forschungsbericht*, *LRT-WE-9-FB-4*, 2003.

Hennig, T., Präzise Positionsbestimmung der Bodenstationen des DSN und der ESA, Diplomarbeit am Institut für Raumfahrtechnik an der Universität der Bundeswehr, München, 2008.

Hull, T. E., W. H. Enright, B. M. Fellen and A. E. Sedgwick, Comparing Numerical Methods for Ordinary Differential Equations, *SIAM J. Numer. Anal.*, *9*, 603–637, 1972.

IERS, International Earth Rotation and Reference Systems Service, http://itrf.ensg.ign.fr, 2009.

Ifadis, I., The Atmospheric Delay of Radio Waves: Modeling the Elevation Dependence on a Global Scale, *Technical Report no. 38L*, 1986.

Janes, H. W., R. B. Langley and S. P. Newby, Analysis of tropospheric delay prediction models - Comparisons with ray-tracing and implications for GPS relative positioning, *Bulletin Geodesique*, *65*, 151–161, 1991.

Juup, D. L. B. and K. Vozoff, Stable Iterative Methods for the Inversion of Geophysical Data, *J. Geophys. Res.*, *42*, 957–976, 1975.

Kautzleben, H., Kugelfunktionen, in *Geomagnetismus und Aeronomie*, edited by G. Fanselau, B. G. Teubner, Leipzig, 1965.

Kertz, W., *Einführung in die Geophysik*, vol I und II, Spektrum Akademischer Verlag, Heidelberg, Berlin, Oxford, 1995.

Klobuchar, J. A., A First Order, Worldwide, Ionospheric, Time-Delay Algorithm, *Air Force Surveys in Geophysics*, *324*, 1975.

Kopka, H., *Latex, Einführung*, Addison-Wesley Verlag, München, 2000.

Lipschutz, S., *Lineare Algebra*, McGraw-Hill Company Europe, London, 4. Auflage, 1990.

McCarthy, D. D. and G. Petit, IERS Conventions (2003), *International Earth Rotation and Reference System Service (IERS)*, *IERS Technical Note; N0. 32*, 2003.

Mendes, V. B. and R. B. Langely, A Comprehensive Analysis of Mapping Functions Used in Modeling Tropospheric Propagation Delay in Space Geodetic Data, in *International Symposium on Kinematic Systems in Geodesy, Geomatics and Navigation*, 1994.

Mendes, V. B. and R. B. Langely, Tropospheric Zenith Delay Prediction Accuracy for Airborne GPS High-Precision Positioning, in *Proceedings of The Institute of Navigation 54th Annual Meeting*, 337–347, Juni 1998.

Milani, A., A. Nobili and P. Farinella, *Non-gravitational perturbations and satellite geodesy*, IOP Publishing Ltd, Bristol, 1. Auflage, 1987.

Montenbruck, O. and E. Gill, *Satellite Orbits*, Springer, New York, Berlin, 2000.

Morabito, D. D. and S. W. Asmar, Radio-Science Performance Analysis Software, *TDA Progress Report*, *42-120*, 1995.

Morley, T., Optical properties of the Rosetta spacecraft, Personal Communication, 2008.

NAIF, The NASA Planetary Science Division's Ancillary Information System SPICE, http://naif.jpl.nasa.gov/naif/, 2009.

Parkinson, B. W. and H. J. Spilker, *Global Positioning System: Theory and Applications*, vol I, American Institute of Aeronautics and Astronautics, 2. Auflage, 1996.

Pätzold, M., Mars Express Orbiter Radio Science MaRS: Flight Operations Manual - Experiment User Manual, MEX-MRS-IGM-MA-3008 , Issue 2, Revision 1, 2003.

Pätzold, M., IFMS Doppler Processing Software: Level 1a to Level 2 Software Design Specifications, MEX-MRS-IGM-DS-3035, Issue 2, Revision 4, 2004.

Pätzold, M., Rosetta Radio Science Investigations Experiment User Manual, RO-RSI-IGM-MA-3081, Issue 4, Revision draft, 2006.

Pätzold, M., F. M. Neubauer et al., MaRS: Mars Express Orbiter Radio Science, in *Mars Express, The Scientific Payload*, edited by A. W. E. P. Division, 141–164, ESA, ESA Publ. Division, 2004.

Press, W. H., S. A. Teukolsky, W. T. Vetterling and B. P. Flannery, *Numerical Recipes in Fortran*, Cambridge Univ. Press, Cambridge, 2. Auflage, 1986.

Remus, S., B. Häusler, M. Pätzold and A. Wennmacher, Ergebnisse der Radio Science Testmessungen an den ESA-Satelliten Rosetta und Mars Express, *DGLR Jahrestagung Hamburg*, 2001.

Saastamoinen, J., Atmospheric Correction for the Troposphere and Stratosphere in Radio Ranging Satellites, in *The Use of Artificial Satellites for Geodesy*, edited by S. W. Henriksen and others, 247–252, American Geophysical Union, Washington D. C., 1972.

Schaer S., How to use CODE's Global Ionosphere Maps, ftp://ftp.unibe.ch/aiub/ionosphere/doc/, 1997.

Schneider, M., *Satellitengeodäsie*, BI-Wissenschafts-Verlag, Mannheim, Wien, Zürich, 1988.

Schwinger, J., Simulation von Umlaufbahnen um einen Kometenkern, Diplomarbeit am Institut für Geophysik und Meteorologie an der Universität zu Köln, 2001.

Seidelmann, P. K. and T. Fukushima, Why new time scales, *Astron. Astrophys.*, *265*, 833 – 838, 1992.

Seidelmann, P. K. et al., Report of the IAU/IAG Working Group on Cartographic Coordinates and Rotational Elements of the Planets and Satellites:2000, *Cel. Mech. and Dynam. Astron.*, *82*, 83–110, 2001.

Selle, J., Planung und Simulation von Radio-Science-Experimenten interplanetarer Raumfahrt-Missionen, Dissertation am Institut für Raumfahrtechnik an der Universität der Bundeswehr, München, 2005.

Smith, S. W., *The Scientist Engineer's Guide to Digital Signal Processing*, California Technical Pub, 1998.

Soffel, M. H., *Relativity in Astrometry, Celestial Mechanics and Geodesy*, Springer-Verlag, Berlin, Heidelberg, 1989.

Stiffel, A. K., Untersuchung verschiedener numerischer Filterverfahren zur Verbesserung des Signal- zu Rauschverhältnis bei Schwerefeldmessung von Mars Express, Studienarbeit II am Institut für Raumfahrtechnik an der Universität der Bundeswehr, München, 2008.

Vallado, D. A., *Fundamentals of Astrodynamics and Applications*, Space Technology Library, Dordrecht, Boston, London, 2001.

Yuen, J. H., *Deep Space Telecommunications System Engineering*, Plenum Press, New York and London, 1983.